LASER SCATTERING BY AEROSOLS OF SMOKE AND COSMETIC SPRAYS

Dissertation submitted to the Jawaharlal Nehru University
in partial fulfilment of the requirements for
the award of the Degree of
MASTER OF PHILOSOPHY

By
RAVINDRA PRATAP SINGH

SCHOOL OF ENVIRONMENTAL SCIENCES
JAWAHARLAL NEHRU UNIVERSITY
NEW DELHI—110067. INDIA
JULY, 1988

CERTIFICATE

Certified that the work reported in this dissertation entitled **"Laser Scattering By Aerosols Of Smoke And Cosmetic Sprays"** has been carried out in the School of Environmental Sciences, Jawaharlal Nehru University, New Delhi. The work is original and has not been submitted in part or in full for any other degree or diploma in this or any other University.

RAVINDRA PRATAP SINGH

(CANDIDATE)

DR. V.K.JAIN

(SUPERVISOR)

JULY

1988

PROF. L.K. PANDE

(DEAN)

SCHOOL OF ENVIRONMENTAL SCIENCES

JAWAHARLAL NEHRU UNIVERSITY

NEW DELHI - 110 067 (INDIA)

Dedicated

to

Rajan Bhaiia

ACKNOWLEDGEMENT

The work contained in the present thesis is suggested and guided by my supervisor, Dr. V.K. Jain. I feel great pleasure in expressing my sense of gratitude and thankfulness for his persistent guidance, encouragement and delightful discussions.

I take this opportunity to acknowledge the kind hospitality of Dr. S. Chopra, I.I.T. Delhi, in providing his lab to learn some aspects of photocorrelation technique. His lectures have helped me a lot in understanding the photo-correlation. Again, I would not be doing justice if I fail in recording my gratitude to Mr. B. Devraj and Mr. B.P. Singh, research students of Prof. Chopra, who took pains to demonstrate and elaborate the photon correlation spectroscopy in their lab.

I don't think that words can be sufficient to acknowledge the help and guidance of my elder brother Rajan Bhaia without whom I would not have been able to to this work. At the sametime, I give my thanks to my labmates and friends Dr. D.V. Rai, Rajkumar, Awadesh, Hari Ram, Shakun, Anwar, Chandrashekhar Mahapatra, S. Konar and many others who helped me at several stages of my work. Thanks are also due for all those who loved and inspired me to think and work.

I am thankful to Mr. Gajanan for typing the manuscript.

Finally I would like to thank Dean, SES, JNU, and C.S.I.R. for providing me the facilities and financial assistance to carry out my research.

Ravindra Pratap Singh

CONTENTS

CHAPTER - I

INTRODUCTION

A variety of disperse systems constitute our environment. The well known examples are colloids and aerosols. Colloids are characterized by homogeneous liquid media with dispersed particles and aerosols with a gaseous medium in which the liquids (fog, mist, etc.) or solid substances (dust, smoke, etc.) may be dispersed. Classification of aerosols can be made under two headings: (i) Dispersion aerosols, which are formed by atomisation of solids and liquids and; (ii) condensation aerosols, formed by condensation of super saturated vapour or due to chemical reaction in the gas phase.

Size and shape of the dispersed particles determine the properties and behaviour of colloids and aerosols. Aerosols in general are polydisperse i.e., the particles have different sizes. Particles having same sizes are termed as monodisperse aerosols. The sizes of colloidal particles vary in the range 1-500 nm. In the case of aerosol particles the sizes are approximately in the range 0.01-100 μm. Particles with sizes greater than 100 μm settle down fast and therefore are not of much interest. Particles of sizes >10 μm affect the visibility and consequently the

biological energy conversion (e.g., photosynthesis). Particles <5-10 μm size can affect health and are of physiological interest. A brief summary of health hazards is given in Appendix 'A'.

Since particle size is the single most important physical parameter which determines the dispersion of aerosols and hence their effect on health, visibility and climate, a great deal of attention has been paid to the studies pertaining to particle size measurements during last couple of decades (e.g., Chu and Churchil, 1955; Cohen et al. 1973; Cowen et al. 1973; Cowen et al. 1981; Pendorff, 1960; Spumy, 1986).

The early work on scattering of light by particles, was initiated by Rayleigh, mainly to study the blueness of sky. For particles having diameter very less than wave-length of light, the scattering - Rayleigh scattering, studies were done by Rayleigh (1918) and Cabannes (1929). Oster (1948) reviewed the work of Rayleigh. Mie (1908) studied the scattering of particles of diameter comparable to wavelength, using Maxwell's equations with appropriate boundary conditions. van de Hulst (1957) gave a good treatment for light scattering by small particles. After this a number of calculations have been done adding

refractive indices and absorption coefficients appropriate to different aerosols.

Scattered intensity distribution for a spherical particle of radius 'r' depends on size parameter $\alpha (= 2\pi r/\lambda)$. For opaque metallic spheres, Geise (1959) and for absorbing spheres relevant to atmospheric scattering by dust particles, Penndorf (1960), Deirmendjian et al. (19610 and Curcio (1961) made the scattering calculations. Olaf and Robock (1961) performed extensive Mie calculations on the angular distribution of light scattered by absorbing spheres, for α = 2, 8, 14, 20 and 26. These calculations covered aerosol particles from 0.3 - 0.5 μm diameter and the range of refractive and absorption indices includes values appropriate to coal and rock dusts. The angular distribution curves of scattered light intensity for opaque particles agree quite closely with curves computed by a simple addition of diffracted and externally reflected light; leaving evaluation by exact Mie theory by Olof et al. (1963). Penndorf (1958, 1959, 1962) described an approximate method of calculating the total scattering coefficient for transparent spheres, which is valid for all particle sizes when $n \leq 2$. Ellison and Peetz (1959) calculated the intensity of scattered light in forward direction using an approximate method applicable to large particles, good enough to be treated by geometrical optics.

Measurements of 90° scattering by plastic latex spheres using polarized light were made by Heller et al. (1962). They evaluated the depolarization ratio. The results obtained using Mie theory agreed well with direct size measurements by electron microscopy.

Experiments on suspended particles (polystyrene latex in water) have been performed by Bateman, Weneck and Eshler (1959). They measured specific extinction using spectrophotometer and calculated the particle size from its variation with the wavelength of light. Angular distribution function based on Mie coefficients have been defined by Chu (1955) and Churchill (1957), which is easier to handle than the usual form involving Mie functions. Angular distribution upto $\alpha = 30$ can be calculated with these functions. Intensity of light scattered by aerosol droplet of diameters between 1.4-3 μm suspended freely between two charged condenser plates have also been measured by Gucker and his associates (1960, 1961). For angles between 40° and 140° from the forward direction, there was good agreement with theoretical intensities calculated from Mie theory.

If the light scattered by one particle is intercepted by other particles, it is called multiple scattering. A

theory for this type of scattering was developed by Churchill and his associates (1955, 1958, 1960). With dense suspensions of monodisperse latex particles (0.8-1.7 μm) satisfactory results were obtained experimentally.

In the above mentioned studies the particles were ass med to be spherical and of uniform size. However, many of the naturally occurring aerosols are of irregular shape and variable size. Stevenson et al. (1961) considered the effect of the particles being unequal in size for α = 25.2. It was found that unimodal and positively skew size distribution can be defined from measurements of depolarization ratio. Methods for finding the size distribution from turbidity measurements at different wavelengths were developed by Wallach et al. (1961). Chin et al. (1955) gave a method of finding size distribution based on the angular variation of the scattered light at very small angles. Experimental data on scattering of fogs has been summarized by Spencer (1960). He developed a scattering function which is valid over a wide range of conditions from thin to dense fogs. At about the same time Went (1960) showed that it is scattering by aerosols of sizes 0.1 μm or less consisting aggregates of condensed molecules, which is responsible for blue atmospheric haze. Experiments with quartz dust suspended in liquid were done.

Ellison (1957) found that the forward scattered light for the quartz dust was approximately the same as scattering calculated for spheres of the same refractive index and the size distribution. Due to assumption of sphericity and transperency of quartz, his results could not be applied immediately to opaque and nonspherical airborne dust. Later Berry (1962) studied the scattering by non-spherical particles, like silver bromide crystals (0.1-1 μm).

In the last two decades a number of studies have been done to determine the sizes of nonspherical particles based on Mie theory, Holland and Guage (1970); Pinnick et al. (1976); Chylek (1977); Zerull et al. (1977); Perry et al. (1978); Janzen (1980). Jaggard et al. (1981) compared the experimental data for latex spheres of regular shape and amonium sulphate and soil dust particle of irregular shape with theoretical Mie calculations. Mie theory was in complete agreement for latex spheres, also applicable to small and resonant sized amonium sulphate particles - not spherical but regular in shape. They concluded that as the particles become larger or more irregular or the particle distribution becomes more peaked the difference between Mie theory calculations and experimental data goes on increasing. Light scattering of a colloidal suspension of iron oxide particles is studied in a very recent experiment by Benzamin

Chu et al. (1987). Their results were consistent with electron microscope measurements.

In view of the scarce data on aerosols of smoke and spray using laser scattering technique, we have attempted to determine the size of aerosols of smoke of cigarettes and cosmetic sprays. In the later part of thesis, we have also reviewed the photon correlatiom technique with a view to determine the particle size.

CHAPTER - II

MIE THEORY

[2.1] INTRODUCTION

Mie gave a general mathematical theory for computing scattering functions that describe the light scattered or absorbed by a particle. Although Mie's theory was formulated for spherical particles, experiments by Napper and Ottewill (1964) and Berry (1962, 1966) indicate that angular scattering patterns and extinction predictions for isometric particles such as cubes or octrahedra differ very little from those for spherical particles of same equivalent size.

[2.2] THEORETICAL ANALYSIS AND DERIVATION OF MIE SCATTERING FUNCTIONS

Mie solved the Maxwell equations for scattering of light by a sphere of diameter comparable to wavelength of incident light using appropriate boundary conditions.

In presence of a medium Maxwell's equations can be expressed in the form of :

$$\vec{\nabla} \times \vec{E} = - \frac{\partial \vec{B}}{\partial t} \qquad (2.1)$$

$$\vec{\nabla} \times \vec{H} = \vec{J} + \frac{\partial \vec{D}}{\partial t} \tag{2.2}$$

$$\vec{\nabla} \cdot \vec{D} = \rho \tag{2.3}$$

$$\vec{\nabla} \cdot \vec{B} = 0 \tag{2.4}$$

where, E is the electric field intensity; D, the dielectric displacement; H, the magnetic field intensity; B, the magnetic induction; J, the current density, and ρ is the charge density.

The field equations are supplemented by the following equations in order to allow a unique determination of the field vectors from a given distribution of current and charge.

$$\vec{J} = \sigma \vec{E} \tag{2.5}$$

$$\vec{D} = \varepsilon \vec{E} \tag{2.6}$$

$$\vec{B} = \mu \vec{H} \tag{2.7}$$

The factors σ, ε and μ are the specific conductance, the electric inductive capacity and magnetic inductive capacity, respectively.

Maxwell's equations are valid for regions of space through which the physical properties of the medium as characterized by σ, ε and μ are continuous. The boundary conditions across the two surfaces are:

(1) The normal component of $\vec{B}$ is continuous

$$(\vec{B}_2 - \vec{B}_1).\vec{n} = 0 \qquad (2.8)$$

(2) There is a discontinuity in the normal component of D equivalent to K, the surface charge density

$$(\vec{D}_2 - \vec{D}_1).\vec{n} = K \qquad (2.9)$$

(3) The tangential component of $\vec{E}$ is continuous

$$(\vec{E}_2 - \vec{E}_1) \times \vec{n} = 0 \qquad (2.10)$$

(4) There is a discontinuity in the tangential component of $\vec{H}$ equal to $\vec{L}$, the surface current density

$$(\vec{H}_2 - \vec{H}_1) \times \vec{n} = \vec{L} \qquad (2.11)$$

From Maxwell's equations one can easily obtain

$$\nabla^2\vec{E} - \sigma \mu \frac{\partial \vec{E}}{t} - \varepsilon \mu \frac{\partial^2 \vec{E}}{\partial t^2} = 0 \qquad (2.12)$$

and

$$\nabla^2\vec{H} - \sigma\mu\frac{\partial\vec{H}}{\partial t} - \mu\varepsilon\frac{\partial^2\vec{H}}{\partial t^2} = 0 \qquad (2.13)$$

In nondissipative media, where $\sigma = 0$, the second term drops out and we have

$$\nabla^2\vec{E} - \varepsilon\mu\frac{\partial^2\vec{E}}{\partial t^2} = 0 \qquad (2.14)$$

and

$$\nabla^2\vec{H} - \varepsilon\mu\frac{\partial^2\vec{H}}{\partial t^2} = 0 \qquad (2.15)$$

Now we proceed directly to the exact solution of the scattering of a plane electromagnetic wave by an isotropic, homogeneous sphere of arbitrary size.

Whenever a plane wave is incident upon an object possessing a discrete boundary and with optical constants different from those of medium, a scattered wave is generated. The field vectors which describe the electromagnetic properties of space may be resolved into three parts - the incident wave $\vec{E}_i$, $\vec{H}_i$, the wave inside the particle, $\vec{E}_r$, $\vec{H}_r$ and the scattered wave $\vec{E}_s$, $\vec{H}_s$. These quantities satisfy the vector wave equations (2.12) and (2.13). A particular solution of the vector wave equation is sought for which the field inside the object, $\vec{E}_r$, $\vec{H}_r$ and

the external field, $\vec{E}_i+\vec{E}_s$, $\vec{H}_i+\vec{H}_s$, satisfy the boundary conditions formulated by (2.8) to (2.11). Once this solution is obtained, not only is the scattered wave completely defined, but the electromagnetic conditions inside within the object are known as well. For a sphere, spherical coordinates r, θ, Φ provide a natural coordinate system. Geometry of scattering is shown in Fig.(2.1). Rather than dealing directly with the vector wave equation (2.12) and (2.13), it is possible to work with the scalar wave equation (2.16)

$$\nabla^2 u - \sigma\mu \frac{\partial u}{\partial t} - \varepsilon\mu \frac{\partial^2 u}{\partial t^2} = 0 \qquad (2.16)$$

where , the scalar quantity u may represent one of the components of $\vec{E}$ or $\vec{H}$.

One device is to introduce two auxiliary functions, the electric Hertz vector, $\vec{\pi}_1$, and the magnetic Hertz vector, $\vec{\pi}_2$, which may be defined by

$$B_1 = \mu \varepsilon \vec{\nabla} \times \partial \vec{\pi}_1 / \partial t \qquad (2.17)$$

$$E_1 = \vec{\nabla}, \vec{\nabla} , \vec{\pi}_1 - \mu \varepsilon \partial^2 \vec{\pi}_1 / \partial t^2 \qquad (2.18)$$

$$D_2 = - \mu \varepsilon \vec{\nabla} \times \partial \vec{\pi}_2 / \partial t \qquad (2.19)$$

$$H_2 = \vec{\nabla}. \vec{\nabla} . \vec{\pi}_2 - \mu \varepsilon \nabla^2 \vec{\pi}_2 / \partial t^2 - \sigma \mu \vec{\pi}_2 \qquad (2.20)$$

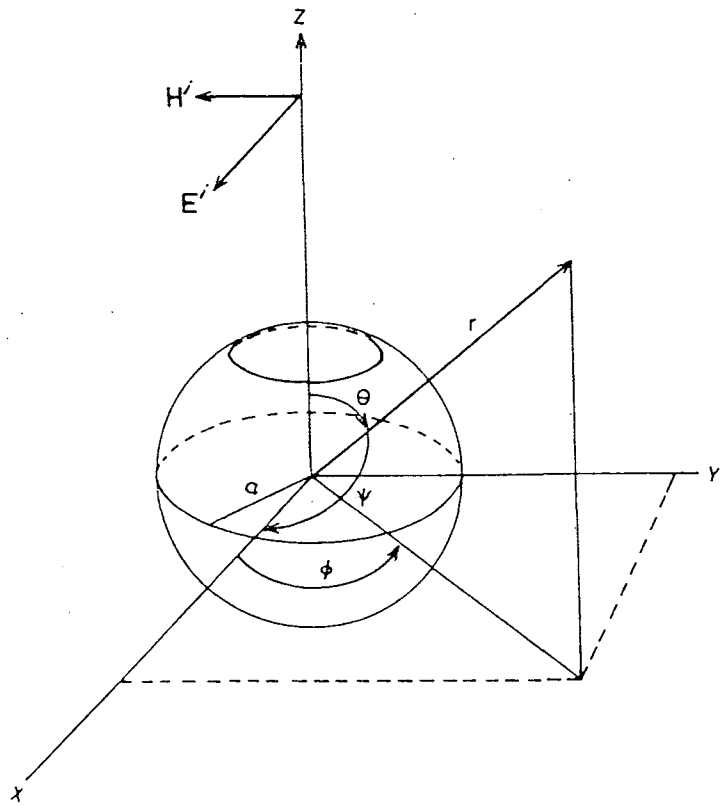

Fig. 2.1: Geometry for scattering. Incident wave travels along positive z-axis with electric vector polarized along x-axis. Particle with radius a has its center at the origin. Direction of scattered wave is defined by polar angles θ and ϕ .

These π_1 and π_2 satisfy the following forms of the vector wave equation:

$$\nabla^2 \pi_1 - \sigma\mu \frac{\partial \pi_1}{\partial t} - \varepsilon_o\mu \frac{\partial^2 \pi_1}{\partial t^2} = - \frac{\vec{P}}{\varepsilon_o} \qquad (2.21)$$

$$\nabla^2 \pi_2 - \sigma\mu_o \frac{\partial \pi_2}{\partial t} - o \frac{\partial^2 \pi_2}{\partial t^2} = - \vec{M} \qquad (2.22)$$

where $\vec{P}$ and $\vec{M}$, the electric and magnetic polarization vectors are defined as:

$$\vec{P} = \vec{D} - \varepsilon_o \vec{E} \qquad (2.23)$$

$$\vec{M} = \left(\frac{1}{\mu_o}\right) \vec{B} - \vec{H} \qquad (2.24)$$

and arise from respective distributions of electric and magnetic dipoles. ε_o, μ_o are the free space inductive capacities.

The Hertz vectors can be defined as:

$$- \vec{\nabla} \cdot \vec{\pi}_1 = \pi_1 \qquad (2.25)$$

$$- \vec{\nabla} \vec{\pi}_2 = \pi_2 \qquad (2.26)$$

where π_1 and π_2, the Hertz Debye potentials, are solutions of the scalar wave equation.

In terms of the Debye potentials, the components of the field vectors in spherical coordinates are given by (Kerker, 1969).

$$E_r = E_{1r} + E_{2r} = \frac{\partial^2 (r\,\pi_1)}{\partial r^2} + K^2 r\,\pi_1 + 0 \qquad (2.27)$$

$$E_\theta = E_{1\theta} + E_{2\theta} = \frac{1}{2}\,\frac{\partial^2 (r\pi_1)}{\partial r\,\partial\theta} + K_2\,\frac{1}{r\sin\theta}\,\frac{\partial (r\,\pi_2)}{\partial\phi} \qquad (2.28)$$

$$E_\phi = E_{1\phi} + E_{2\phi} = \frac{1}{r\sin\theta}\,\frac{\partial^2 (r\pi_1)}{\partial r\,\partial\phi} - K_2\,\frac{1}{r}\,\frac{\partial (r\,\pi_2)}{\partial\theta} \qquad (2.29)$$

$$H_r = H_{1r} + H_{2r} = 0 + \frac{\partial^2 (r\,\pi_2)}{\partial r^2} + K^2\,r\,\pi_2 \qquad (2.30)$$

$$H_\theta = H_{1\theta} + H_{2\theta} = -K_1\,\frac{1}{r\sin\theta}\,\frac{\partial (r\pi_1)}{\partial\phi} + \frac{1}{r}\,\frac{\partial^2 (r\pi_2)}{\partial r\,\partial\theta} \qquad (2.31)$$

$$H_\phi = H_{1\phi} + H_{2\phi} = K_1\,\frac{1}{r}\,\frac{\partial (r\pi_1)}{\partial\theta} + \frac{1}{r\sin\theta}\,\frac{\partial^2 (r^2\,\pi_2)}{\partial r\,\partial\phi} \qquad (2.32)$$

where the propagation constant

$$K^2 = -\,K_1\,K_2 \qquad (2.33)$$

$$K_1 = i\omega\varepsilon + \sigma \qquad (2.34)$$

and

$$K_2 = i\omega \qquad (2.35)$$

since all media are considered to be nonmagnetic has been dropped.

For sinusoidal time dependence, e^{iwt}, the non-homogeneous scalar wave equation(2.16) reduces to the homogeneous form:

$$\nabla^2 u' + K^2 u' = 0 \qquad (2.36)$$

where

$$u = u' e^{iwt} \qquad (2.37)$$

The Hertz-Debye potentials are solutions of this equation, which can be solved by method of separation of variables. In spherical coordinates, the wave equation becomes

$$\frac{1}{r}\frac{\partial^2 r\pi}{\partial r^2} + \frac{1}{r^2 \sin\theta}\frac{\partial}{\partial\theta}\left(\sin\theta \frac{\partial\pi}{\partial\theta}\right) + \frac{1}{\sin^2\theta}\frac{\partial^2\pi}{\partial\phi^2} + K^2\pi = 0 \qquad \ldots\ldots (2.38)$$

Here the exponential time factor has been factored out of the potential function.

By variable separable method we get the general solution as

$$r\pi = \sum_{n=0}^{\infty}\sum_{m=-n}^{n} \{C_n \Psi_n(Kr) + d_n \chi_n(Kr)\}\{P_n^{(m)}(\cos\theta)\}$$

$$\{a_m \cos(m\phi) \; b_m \sin(m\phi)\} \qquad (2.39)$$

where Ψ_n, χ_n are Ricatti-Bessel functions and $P_n^{(m)}$ is associated legendre polynomial.

The isotropic homogeneous sphere is characterized by a propogation constant K_1 which may or may not be complex. The isotropic homogeneous medium will be considered to be a dielectric so that its propagation constant, K_2 is real. The ratio of these quantities defines the relative refractive index.

$$m = K_1/K_2 = m_1K_0//m_2K_0 = m_1/m_2 \tag{2.40}$$

The particle of radius a is located at the origin of the spherical coordinate system so that its boundary corresponds to the constant cordinate surface, r = a. The geometry is shown in Fig. 2.1. The plane polarized wave propagating along the positive Z-axis, has its electric vector of unit amplitude along X-axis.

$$\vec{E}^i = |\exp(-iK_2Z)| = 1 \tag{2.41}$$

when this is expanded in the form of equation (2.39), it becomes

$$r\,\pi_1^i = \frac{1}{K_2^2} \sum_{n=1}^{\infty} i^{n-1} \frac{2n+1}{n(n+1)} \Psi_n(K_2r)\, P_n^{(1)}(\cos\theta)\cos\phi \tag{2.42}$$

$$r\,\pi_2^{i} = \frac{1}{K_2^2}\sum_{n=1}^{\infty} i^{n-1}\,\frac{2n+1}{n(n+1)}\,\Psi_n(K_2r)\,P_n^{(1)}(\cos\theta)\,\sin\phi \qquad (2.43)$$

where $P_n^{(1)}(\cos\theta)$ is the associated legendre function of the first kind. The functions $\chi_n(K_2r)$ have been dropped from this expression since they become infinite at the origin through which the incident wave must pass. Therefore, only the Ricatti-Bassel function $\Psi_n(K_2r)$ is utilized. The above equations describe the unperturbed incident wave.

In order to match these potentials with those of the internal and scattered waves, the latter must be expressed in a series of similar form but with arbitrary coefficients. Again, only the function $\Psi_n(K_1r)$ may be used in the expression for the potential inside the particle since $\chi_n(K_1r)$ becomes infinite at the origin. On the other hand, the scattered wave must vanish at infinity and the Hankel functions, $\zeta_n(K_2r)$ $[=\Psi_n(K_2r) + i\,\chi_n(K_2r)]$ will impart precisely this property. Accordingly, it will be used in the expression of the scattered wave, so that

$$r\,\pi_1^{s} = \frac{1}{K_2^2}\sum_{n=1}^{\infty} i^{n-1}\,\frac{2n+1}{n(n+1)}\,a_n\zeta_n(K_2r)P_n^{(1)}(\cos\theta)\cos\phi \qquad (2.44)$$

$$r\,\pi_2^{s} = \frac{1}{K_2^2}\sum_{n=1}^{\infty} i^{n-1}\,\frac{2n+1}{n(n+1)}\,b_n\zeta_n(K_2r)\,P_n^{(1)}(\cos\theta)\sin\phi \qquad (2.45)$$

and

$$r\,\pi_1^r = \frac{1}{K_1^2}\sum_{n=1}^{\infty} i^{n-1}\,\frac{2n+1}{n(n+1)}\,c_n\,\Psi_n(K_1 r)\,P_n^{(1)}(\cos\theta)\cos\phi \quad (2.46)$$

$$r\,\pi_1^r = \frac{1}{K_1^2}\sum_{n=1}^{\infty} i^{n-1}\,\frac{2n+1}{n(n+1)}\,c_n\,\Psi_n(K_1 r)\,P_n^{(1)}(\cos\theta)\sin\phi \quad (2.47)$$

The boundary conditions are that the tangential components of E & H be continuous across the spherical surface r = a. From (2.27) through (2.32), it is apparent that for the Debye potential it is equivalent to

$$\left(\frac{\partial}{\partial r}\right)\left[r(\pi_1^i + \pi_1^s)\right] = \left(\frac{\partial}{\partial r}\right)\left[r\,\pi_1^r\right] \quad (2.48)$$

$$\left(\frac{\partial}{\partial r}\right)\left[r(\pi_2^i + \pi_2^s)\right] = \left(\frac{\partial}{\partial}\right)\left[r\,\pi_2^r\right] \quad (2.49)$$

$$K_1^{(2)} r\,(\pi_1^i + \pi_1^s) = K_1^{(1)}\,r\,\pi_1^r \quad (2.50)$$

$$K_2^{(2)} r\,(\pi_2^i + \pi_2^s) = K_2^{(1)}\,r\,\pi_2^r \quad (2.51)$$

which give

$$m\left[\Psi_n'(K_2 a) - a_n\,\zeta_n'(K_2 a)\right] = C_n\,\Psi_n'(K_1 a) \quad (2.52)$$

$$m\left[\Psi_n'(K_2 a) - b_n\,\zeta_n'(K_2 a)\right] = d_n\,\Psi_n'(K_1 a) \quad (2.53)$$

$$\psi_n(K_2a) - a_n \zeta_n(K_2a) = C_n \psi_n(K_1a) \qquad (2.54)$$

$$m^2 [\psi_n(K_2a) - b_n \zeta_n(K_2a)] = d_n \psi_n(K_1a) \qquad (2.55)$$

The relative complex refractive index of the sphere appears in these equations through its relation to the propagation constants by

$$K_1 = m_1 K_o; \quad K_1^{(1)} = i m_1^2 K_o; \quad K_2^{(1)} = i K_o \qquad (2.56)$$

and

$$K_2 = m_2 K_o; \quad K_2^{(1)} = i m_2^2 K_o; \quad K_2^{(2)} = i K_o \qquad (2.57)$$

where, as usual, $K_o = 2\pi / \lambda_o$ is the propagation constant in free space.

These equations can now be solved for the four sets of coefficients a_n, b_n, c_n and d_n. Only the first two are of interest here, and these are given by

$$a_n = \frac{\psi_n(\alpha)\psi_n'(\beta) - m\psi_n(\beta)\psi_n'(\alpha)}{\zeta_n(\alpha)\psi_n'(\beta) - m\psi_n(\beta)\zeta_n'(\alpha)} \qquad (2.58)$$

$$b_n = \frac{m\psi_n(\alpha)\psi_n'(\beta) - \psi_n(\beta)\psi_n'(\alpha)}{m\zeta_n(\alpha)\psi_n'(\beta) - \psi_n(\beta)\zeta_n'(\alpha)} \qquad (2.59)$$

where $\alpha = K_2 a = 2\pi m_2 a / \lambda_o$ (2.60)

$$\beta = K_1 a = 2\pi m_1 a / \lambda_o \qquad (2.61)$$

α is called size parameter.

Here λ_o is the wavelength in vacuo, λ is the wavelength in the medium and $m=m_1/m_2$ is the refractive index of the particle relative to that of the medium. The addition of a prime to the Ricatti-Bessel functions denotes differentiation with respect to their arguments.

We now consider the scattered field at distances sufficiently far from the particle so that $K_2 r >> n$ where n is the order of Ricatti-Bassel function. The Hankel functions in (2.44) and (2.45) reduce as follows:

$$\zeta_n (K_2 r) = i^{(n+1)} \exp(-iK_2 r) \tag{2.62}$$

and

$$\zeta_n'(K_2 r) = i^n \exp(-iK_2 r) \tag{2.63}$$

A further simplification in the far-field zone results from the scattered wave becoming a transverse wave as a result of the rapid decay of the longitudinal component. The transverse components of the field vectors (E_θ , E_ϕ , H_θ , H_ϕ _ decay with λ/r in accordance with inverse square dependence of a spherical wave upon the radial distance. The radial components E_r and H_r fall off as $(\lambda/r)^2$ so that they may be neglected in the far-field zone. The final result is:

$$E_\phi = \frac{H_\theta}{(m_2)} = -\frac{i \exp(-iK_2 r)}{K_2} \sin\phi \sum_{n=1}^{\infty} \frac{2n+1}{n(n+1)}$$

$$x \{ a_n \frac{P_n^{(1)}(\cos\theta)}{\sin\theta} + b_n \frac{dP_n^{(1)}(\cos\theta)}{d\theta} \quad (2.64)$$

$$E = \frac{H_\phi}{(m_2)} = - \frac{i \exp(-iK_2 r)}{K_2} \cos\phi \sum_{n=1}^{\infty} \frac{2n+1}{n(n+1)}$$

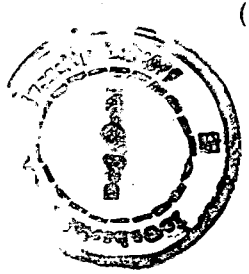

$$x \{ a_n \frac{dP_n^{(1)}(\cos\theta)}{d\theta} + b_n \frac{P_n^{(1)}(\cos\theta)}{\sin\theta} \} \quad (2.65)$$

The inverse dependence upon r indicates that in the radiation zone, the scattered wave is, usual type of spherical wave. Since the phase relation between the two complex quantities E_θ and E_ϕ is arbitrary, the scattered wave will, in general, be elliptically polarized. It will be convenient to designate the quantities in the brackets above as the amplitude functions.

$$S_1 = \sum_{n=1}^{\infty} \frac{2n+1}{n(n+1)} \{ a_n \pi_n(\cos\theta) + b_n \tau_n(\cos\theta) \} \quad (2.66)$$

$$S_2 = \sum_{n=1}^{\infty} \frac{2n+1}{n(n+1)} \{ a_n \tau_n(\cos\theta) + b_n \pi_n(\cos\theta) \} \quad (2.67)$$

where the angular functions are:

$$\pi_n(\cos\theta) = \frac{P_n^{(1)}(\cos\theta)}{\sin\theta} \quad (2.68)$$

$$\tau_n(\cos\theta) = \frac{d}{d\theta} P_n^{(1)}(\cos\theta) \qquad (2.69)$$

Now, using Poynting's theorem, the energy flow in the scattered wave is given by

$$S = 1/2\ (E_\theta\ H_\theta^{*} - E_\phi\ H_\phi^{*}) \qquad (2.70)$$

where the asterisk denotes the complex conjugate. The intensity of scattered radiation polarized in θ and ϕ azimuths is

$$I_\phi = \frac{\lambda^2}{4\pi^2 r^2} |S_1|^2 \sin^2\phi = \frac{\lambda^2}{4\pi^2 r^2} i_i \sin^2\phi \qquad (2.71)$$

$$I_\theta = \frac{\lambda^2}{4\pi^2 r^2} |S_2|^2 \cos^2\phi = \frac{\lambda^2}{4\pi^2 r^2} i_i \cos^2\phi \qquad (2.72)$$

where i_1 and i_2 will be called the intensity functions. These components are perpendicular and parallel, respectively, to the sacttering plane. This plane contains the incident direction and the direction of the scattered wave (θ , ϕ).

There will be a phase difference between these components of the scattered beam given by:

$$\tan \delta = \frac{\mathrm{Re}(S_1)\ \mathrm{Im}(S_2) - \mathrm{Re}(S_2)\ \mathrm{Im}(S_1)}{\mathrm{Re}(S_1)\ \mathrm{Re}(S_2) - \mathrm{Im}(S_1)\ \mathrm{Im}(S_2)} \qquad (2.73)$$

where Re and Im designate the real and imaginary parts of the indicated complex amplitude functions.

When yz is chosen as the scattering plane so that the direction of the electric vector of the incident radiation is perpendicular to this plane, $\phi = 90^{\circ}$, and

$$I_{\phi} = I_1 = (\lambda^2/4\ \pi^2\ r^2)\ i_1 \qquad (2.74)$$

On the other hand, with xz as the scattering plane, the incident radiation has its electric vector parallel to the plane $\phi = 0^{\circ}$, and

$$I_{\phi} = I_2 = (\lambda^2/4\ \pi^2\ r^2)\ i_2 \qquad (2.75)$$

So, for unpolarized incident radiation of unit intensity, the intensity of scattered light in the direction θ at a distance from the aerosol particle is given by (Penndorf, 1962a)

$$I(\theta, n) = 1/(2K^2d^2)[i_1(\alpha, \theta, n) + i_2(\alpha, \theta, n) \qquad (2.76)$$

where, n is the refractive index of the medium.

The above result shows that the scattered

radiation is always polarized even if the incident radiation is unpolarized.

And the degree of polarization is given by

$$P = \left| \frac{i_1 - i_2}{i_1 + i_2} \right| \qquad (2.77)$$

The intensity functions derived by Mie are:

$$i_1 = |S_1|^2 = \left| \sum_{}^{\infty} (2m+1) (a_m \pi_m + b_m \tau_m) \right|^2 \qquad (2.78a)$$

$$i_2 = |S_2|^2 = \left| \sum_{}^{\infty} (2m+1) (a_m \tau_m + b_m \pi_m) \right|^2 \qquad (2.78b)$$

Solution of equation (2.78) gives the scattered field as a spherical wave composed of two sets of partial waves, one the electrical wave a_m for which radial component of the magnetic vector in the incident wave is zero and the other magnetic wave b_m for which radial component of electric vector is zero.

Mie coefficient a_m and b_m depend on n, the refractive index and α, the size parameter. The partial wave can be considred as coming from an electric or magnetic multipole field. Hence, the first partial wave comes from a dipole; the second from a quadrupole and so on.

The coefficients π_m and π_m in equation (2.78) denote the angular functions independent of n and α, depending only on the scattering angle θ. Variation of calculated intensity function with the scattering angle for parallel polarization is shown in figs.(2.2)-(2.10), which were obtained by Pinnick et al.(1973) for various values using equation (2.78).

[2.3] APPROXIMATION FORMULAE FOR FORWARD AND SMALL ANGLE SCATTERING

The exact scattering theory gives for the amplitude

$$S\{0\} = \text{Re } S\{0\} + i \text{ Im } S\{0\} \tag{2.79}$$

From equation (2.78), amplitude in forward direction

$$S\{0\} = S_1\{\theta\} = S_2\{\theta\} \tag{2.80}$$

and

$$S_1 = \sum^{\infty} (2m+1) [\pi_m \text{ Re } (a_m) + \tau_m \text{ Re}(b_m) + i \pi_m I_m (a_m) + i \tau_m I_m (a_m)] \tag{2.81}$$

Now, we define two coefficients. First the Angular Mie scattering coefficient

$$i_\theta = (i_1 + i_2)/2\pi\alpha^2 \tag{2.82}$$

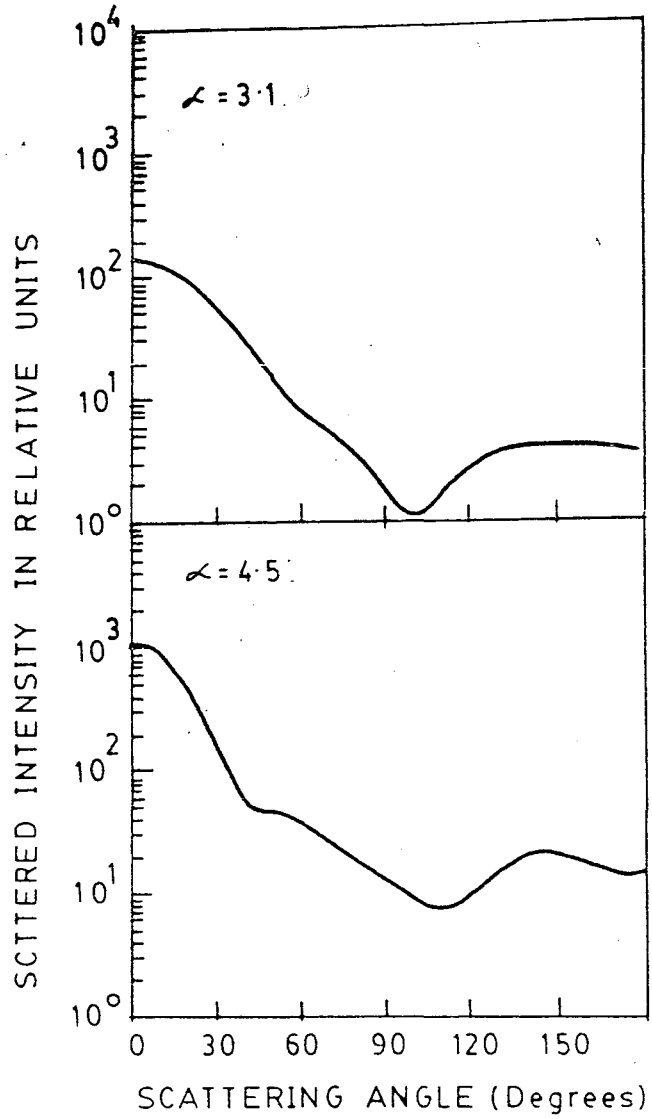

Figs. 2.2 & 2.3: Theoretical plots of scattered intensity as a function of scattering angle from Mie theory calculations for homogeneous spheres for α = 3.1 and 4.5 respectively.

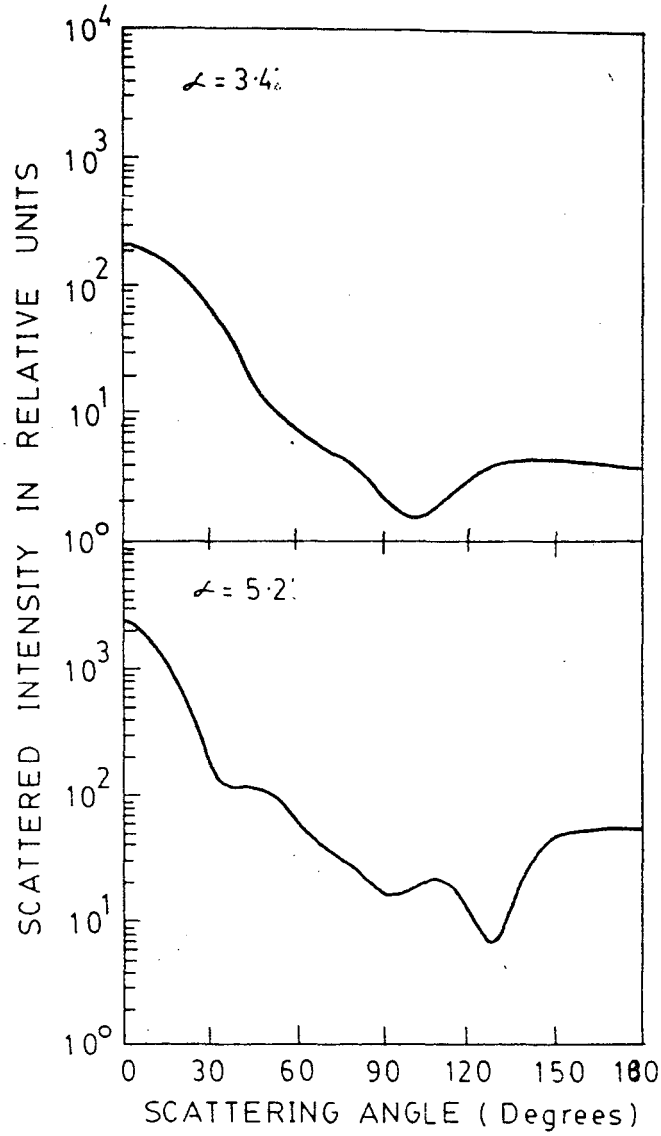

Figs. 2.4 & 2.5: Theoretical plots of scattered intensity as a function of scattering angle from Mie theory calculations for homogeneous spheres for α = 3.4 and 5.2 respectively.

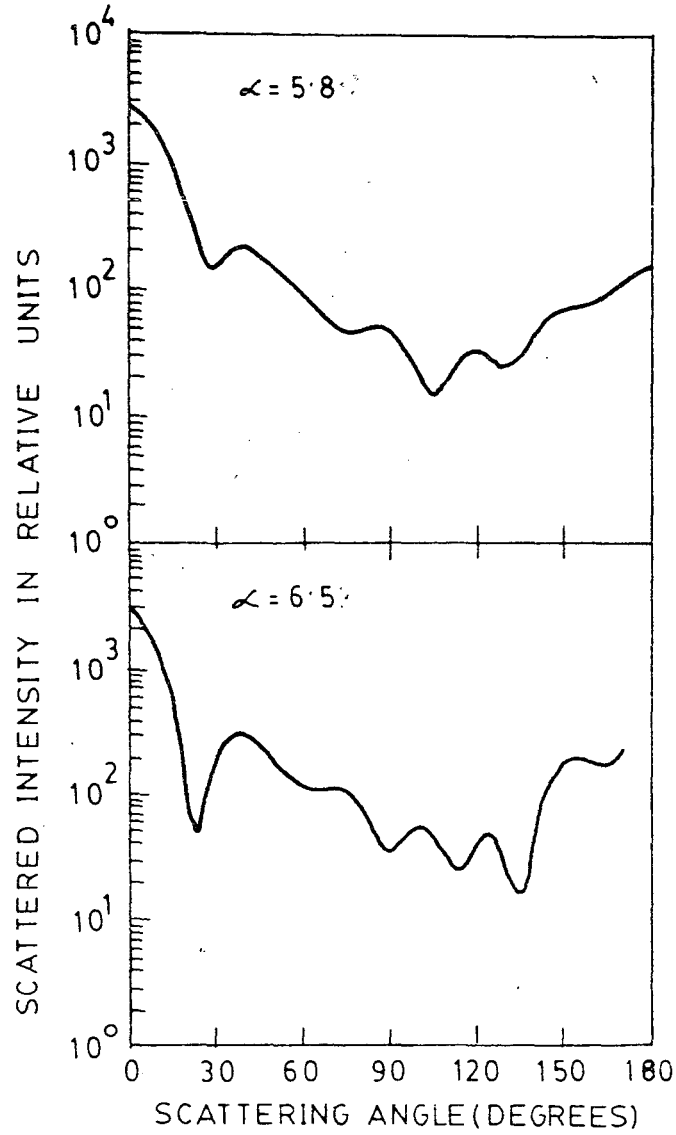

Figs. 2.6 & 2.7: Theoretical plots of scattered intensity Vs. scattering angle from Mie theory calculations for homogeneous spheres for α = 5.8 & 6.5 respectively.

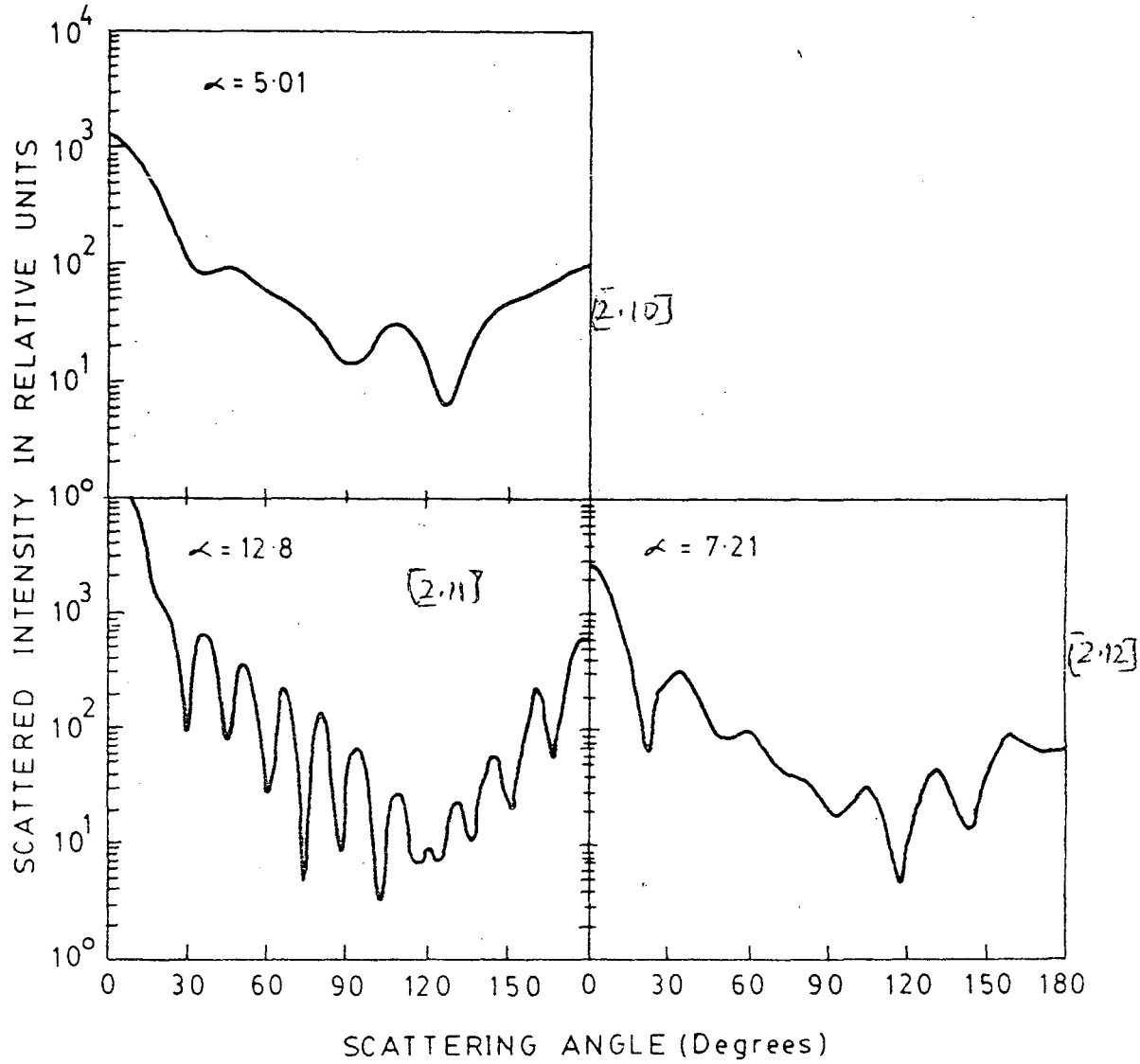

Figs. 2.10, 2.11 & 2.12: Theoretical plots of scattered intensity vs. scattering angle from Mie theory calculations from homogeneous spheres for α= 5.0, 12.8 & 7.2 respectively.

[Figs. 2.4 to 2.12 taken from Pinnick et al. (1973)]

and the second phase function

$$p_m = 2(i_1 + i_2)\ \alpha^2 K \qquad (2.83)$$

According to the cross-section theorem

$$\sigma = \pi r^2\ K^{(e)} = (4\pi/K^2)\ \mathrm{Re}\ S\{0\} = (\lambda^2/\pi)\ \mathrm{Re}\{S(0)\} \qquad (2.84)$$

i.e., the total extinction corss-section is proportional to the real part of the scalar amplitude of the scttering in forward direction. this theorem follows directly from the exact solution of scattering theory and applies to all types of refrative indices (real and imaginary).

In equation (2.84) $K^{(e)}$ denotes the extinction coefficient. For nonabsorbing aerosols

$$K^{(e)} = K$$

i.e., extinction coefficient is identical with the scattering coefficient.

In case of forward scattering,

$$\pi_m = \tau_m = 1/2$$

Since $\mathrm{Re}(a_m)$ and $\mathrm{Re}(b_m)$ consist of positive terms only while $I_m\ (a_m)$ and $I_m(b_m)$ consist of positive and negative terms,

therefore in equation (2.79)

$$| \text{Re } S\{0\} | >> | \dot{I}_m S\{0\} | \qquad (2.85)$$

This inequality is true only for above a certain lower limit.

For $\alpha > 5$, $I_m S\{0\}$ becomes negligible.

Hence,

$$S_1' = \text{Re } S\{0\} \qquad (2.86)$$

Prime indicates that parameters are based on validity of euqation (2.85).

The approximated intensity function is obtained by inserting equation (2.86) into equation(2.79)

$$i_1' = i_2' = | \text{Re } S_1\{0\} |^2 = | \text{Re } S_2\{0\} |^2 \qquad (2.87)$$

From the cross-section theorem

$$\frac{1}{4} \alpha^2 K = \text{Re } S\{0\} \qquad (2.88)$$

Replacing Re $S\{0\}$ in equation (2.87) by left hand side of equation (2.70) gives

$$i_1' = i_2' = (1/4\ \alpha^2 K)^2 \quad (\frac{1}{4}\alpha^2 K)^2 \qquad (2.89)$$

Using the definition given in equation (2.80) equation (2.89) follows

$$i_{\theta}' = \alpha^2 K^2/16\pi \qquad (2.90)$$

Therefore from equation (2.81)

$$p_M' = 1/4\ \alpha^2 K \qquad (2.91)$$

P_M' is called approximated phase function. K approaches the value 2 for very large α and the relationship expressed by equation (2.69) becomes

$$\lim_{\alpha\to\infty} P_M' = 1/2\ \alpha^2 \qquad (2.92)$$

which is in perfect agreement with diffraction theory. So for angular variation of scattered intensity at small angles by a sphere, we can write

$$i_1(\theta) = i_1(0)\ \left[\frac{J_1(\alpha \sin\theta)}{\alpha \sin\theta}\right]^2 \qquad (2.93)$$

A number of workers have verified experimentally the Mie theory given above, e.g. LaMer and Sinclair (1943), Gucker and Rowell (1960), Gumprecht and Sliepcevich (1951), Kratohvil and Smart (1965), Michael Lang (1976) and Cowen et al. (1981).

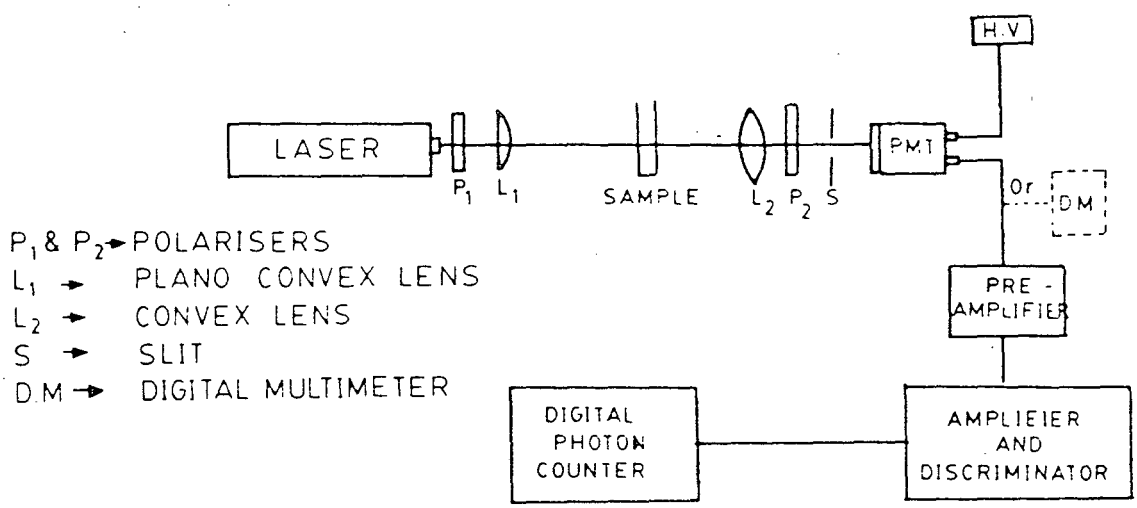

Fig. 3.1: Schematic diagram representing the experimental set up.

CHAPTER III

EXPERIMENTAL SET UP

[3.1] EXPERIMENTAL ARRANGEMENT

The set up which we used for laser light scattering is shown schematically in Fig. (3.1). It consists of mainly three parts, namely a laser source, detection system and a sample mount. A He-Ne laser tube (Melles-Griot) with maximum output power 7 mW was used to produce a laser beam at wavelength λ= 632.8 nm. The detection system comprises of photomultiplier tube (IP-28) in conjunction with a counting system (Preamplifier, amplifier, discriminator, counter) or a digital multimeter. For intensity measurements two types of arrangement were employed. In the first, PMT was followed by a preamplifier (HA505, ECIL) amplifier (PA521, ECIL), discriminator (PD-621, Aplab) and a counter (1101, Aplab). In the second arrangement current from the PMT was measured by a digital multimeter. The sample mount is shown in Fig.(3.2). We have used a polariser (Melles-Griot) to get the parallel polarized light. For a well focussed and perfectly aligned laser beam slit and lenses were used.

The peformance of PM tube with biased voltage is shown in Fig. (3.3). The plateau voltage is found to be 480 V.

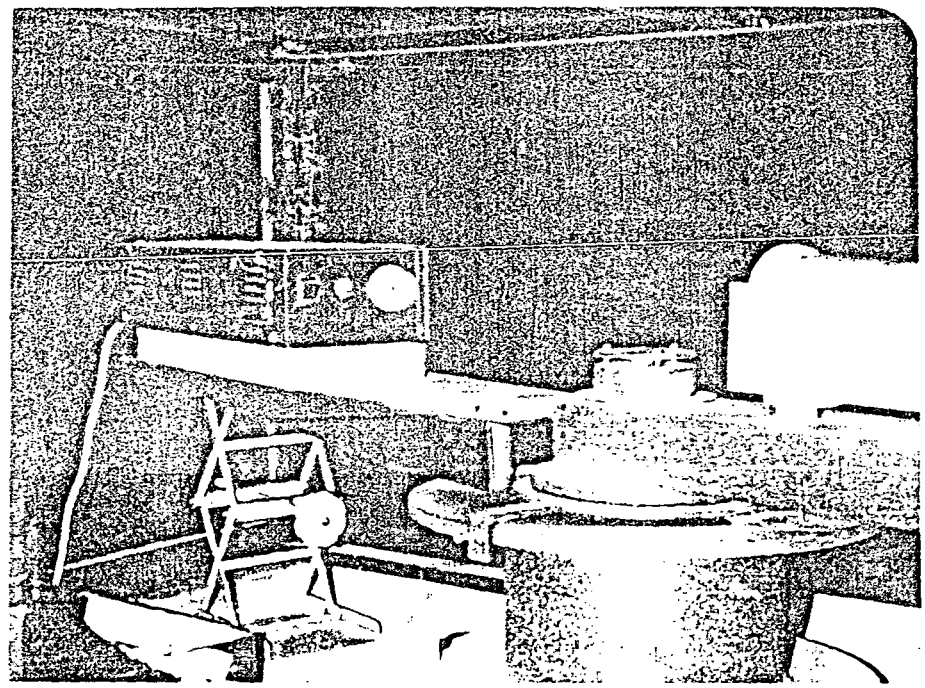

Fig. 3.2: Photograph of Rotating Armed Mount

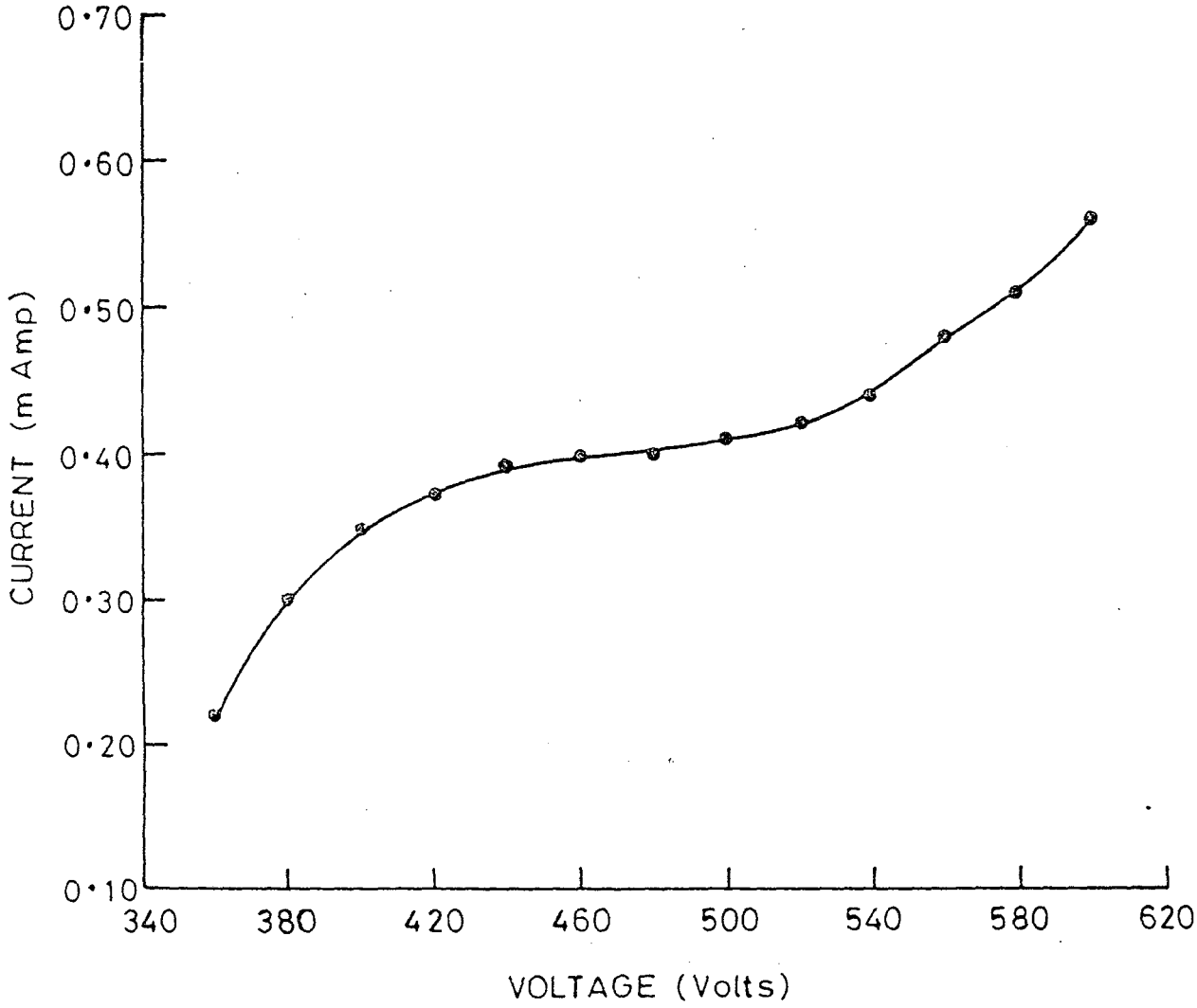

Fig. 3.3: Variation of current with voltage showing the characteristics of the PM tube.

[3.2] Procedure

First the alignment of laser beam is done. For this, levelling of the mount and the arm attached to it was checked by a spirit level. After this, the slits and lenses were used for aligning the laser beam. After alignment, i.e., when the tube is aligned along the incident beam direction (at 0°) laser beam falls on the window of PMT. For focussing the position of lenses were adjusted in such a fashion that the focus lies at the window of PMT for the scattered laser beam.

Every instrument is switched on for 15 to 20 minutes before starting the experiment. PMT is kept at the plateau voltage. PMT takes around thirty minutes to stabilize if it is being used regularly otherwise takes two to three hours.

[3.2.1] Calibration of the Experimental Set up: Now the experimental set up is calibrated for forward scattering approximation theory, which we have used for determining the size of aerosols, by doing experiments with particles of known sizes.

Ferric hydroxide sol was prepared by taking a known weight of ferrous sulphate and boiling it with distilled water for an hour. It was then allowed to cool at the room temperature. The sample thus prepared was diluted 100 times. The Ferric hydroxide sol was chosen because of being

hydrophilic sol which is a good example of idealized problem of separated particles in a homogeneous medium.

The 100 ml of this solution was taken into Attenberg cylinder and diluted again to the mark. It was shaken well and after each interval of time the samples of various sizes were taken out from the cylinder for the scattering experiment. The weight of Ferrous-sulphate was chosen such that after final dilution its concentration should not increase more than 10^{-6} gms/lit.

The sedimentation analysis is based on STOKE'S LAW; which states the law of settling velocity as

$$v = \frac{2}{9} g \frac{D_1 - D_2}{\eta} \cdot r^2$$

where v = particle velocity (cm sec^{-1})

g = Gravity acceleration (981 cm sec^{-2})

D_1 = Density of the falling sphere (gm cm^{-3})

D_2 = Density of the sedimentation liquid (gm cm^{-3})

η = Viscosity of liquid (gm cm^{-1} sec^{-1})

r = Radius of sphere (cm)

Fall time for a given diameter of particle is

$$t = \frac{h}{v}$$

where h = Fall height of suspended column

v = settling velocity for a given diameter in cm/sec.

Keeping the sample suspended in water for a longer time may create problems like coagulation. To check this Hydrogen Peroxide (H_2O_2) was used as dispersant. H_2O_2 affects the substances in two ways. It oxidises the organic materials which often inhibit dispersion. In addition H_2O_2 generates oxygen in the pore space of the substances, which in effect pushes individual particles away from each other. One does not need to keep the trace of concentration of H_2O_2 as on heating it completely dissociates into water and oxygen.

Samples of hydrosols with sizes 2, 3 and 5 microns (i.e., α = 9.92; 14.88 and 24.81) were obtained at various intervals of time using sedimentation technique. The experimentally observed scattered angular intensities as a function of the scattering angle for various paticle sizes (α= 9.9, 14.9 and 24.8) are shown in Figs. (3.4), (3.5), and (3.6). The smooth curves plotted in Figs. (3.4) - (3.6) are obtained from the theoretical calculations of intensities using eqn.(2.95) for α = 9.9, 14.9, 424.8 respectively. The theoretical angular intensity ratio as a function of θ for various values of α are given in Tables (1-6).

From Figs.(3.4)-(3.6) it is evident that the experimental ratios of angular intensities when compared with those obtained from approximation forward scattering

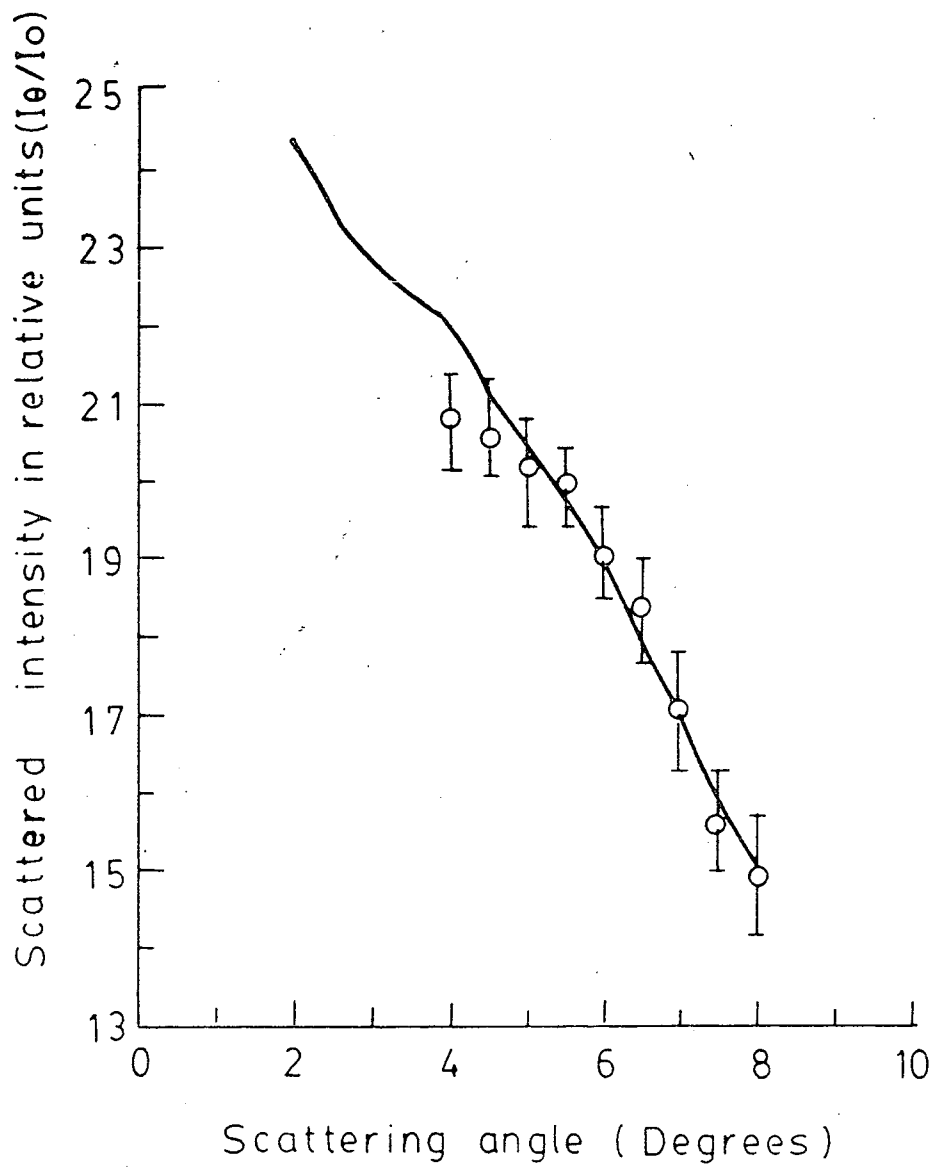

Fig. 3.4: Angular scattering measurements (circles) and approximated forward scattering intensity calculations (smooth curve) for 2 micron ferric hydroxide sols. [$\alpha = 9.9$]

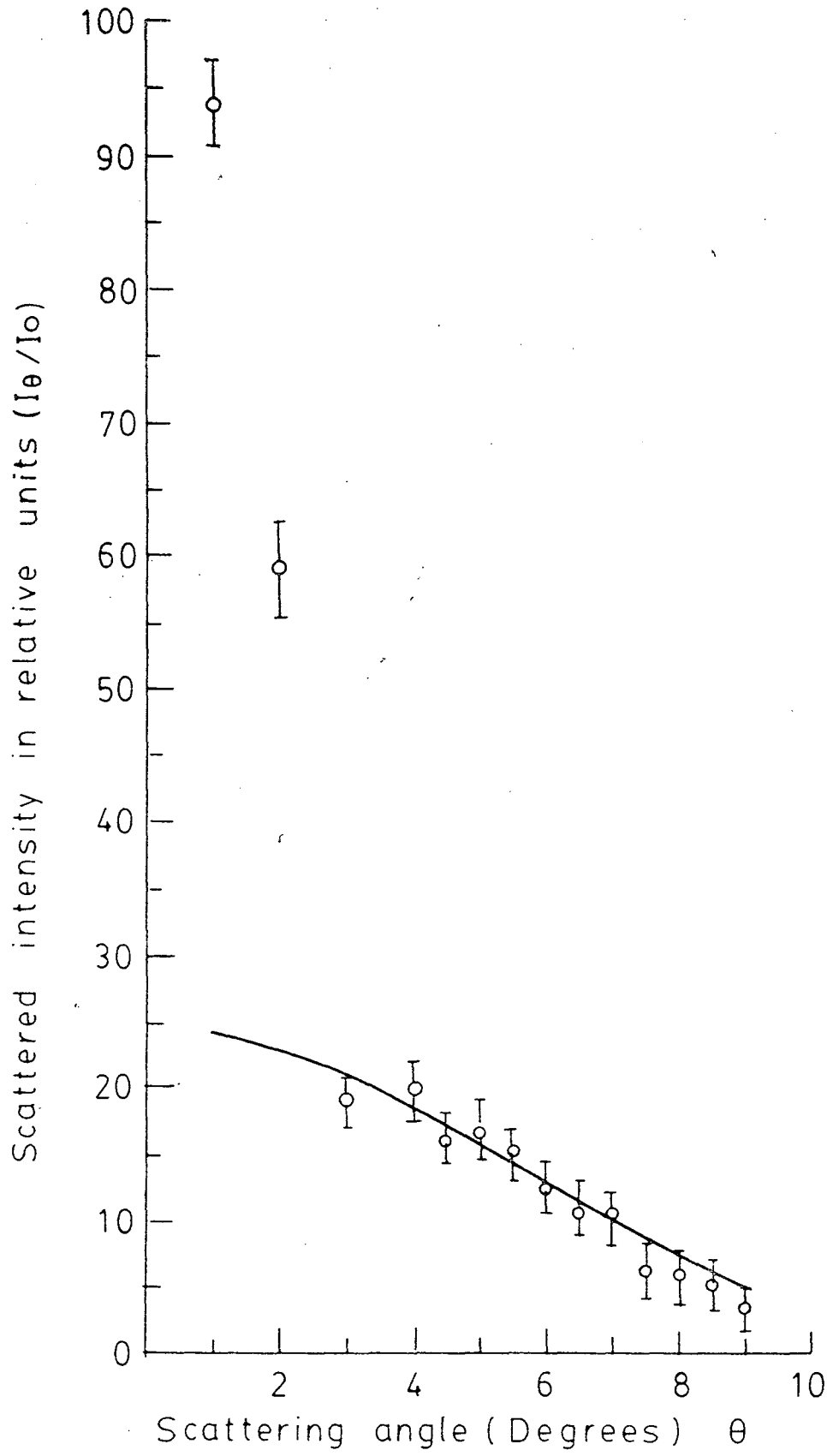

Fig. 3.5: Angular scattering measurements (circles) and approximated forward scattering intensity calculations (smooth curve) for 3 microns ferric hydroxide sols. [$\alpha = 14.9$]

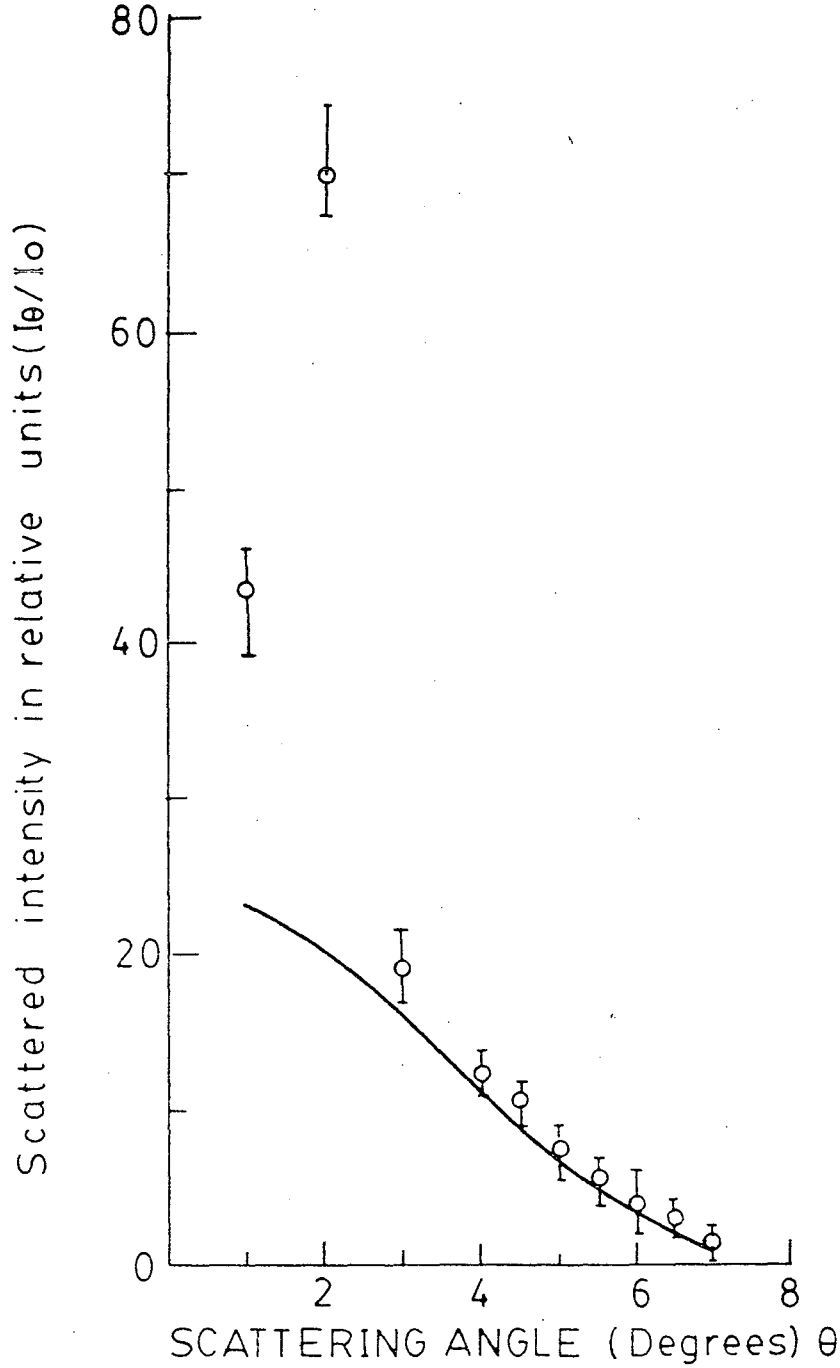

Fig. 3.6: Angular scattering measurements (circles) and approximated forward scattering intensity calculations (smooth curve) for 5 microns ferric hydroxide sols. [$\alpha = 24.8$]

TABLE 1

$[\alpha = 5]$

Angle 'θ' (degrees) [A]	Sin θ [B]	αSin θ [C]	J_1 (αSin θ) [D]	$\frac{J_1(\alpha \sin\theta)}{\alpha \sin\theta}$ [E]	I(θ)/Io [F]
1	0.0174	0.0872	0.04	0.4597	0.2113
2	0.0348	0.1745	0.087	0.4971	0.2471
3	0.0523	0.2617	0.1287	0.495	0.2450
4	0.0697	0.3488	0.172	0.4914	0.2415
5	0.0871	0.4357	0.214	0.4976	0.2476
6	0.1045	0.5226	0.250	0.4807	0.2311
7	0.1218	0.609	0.290	0.4754	0.2260
8	0.1391	0.6595	0.3112	0.4715	0.2223
9	0.1564	0.782	0.360	0.4603	0.2119
10	0.1736	0.868	0.3939	0.4538	0.2059

TABLE 2
[$\alpha = 10$]

[A]	[B]	[C]	[D]	[E]	[F]
1	0.0174	0.174	0.087	0.5	0.25
2	0.0348	0.348	0.172	0.4942	0.2442
3	0.0523	0.523	0.250	0.4780	0.2284
4	0.0697	0.697	0.328	0.4705	0.2214
5	0.0871	0.871	0.3939	0.4522	0.2045
6	0.1045	1.045	0.455	0.4354	0.1895
7	0.1218	1.218	0.503	0.4129	0.1705
8	0.1391	1.391	0.54	0.3882	0.1507
9	0.1564	1.564	0.564	0.3606	0.1300
10	0.1736	1.736	0.578	0.3329	0.1108

TABLE 3

[$\alpha = 15$]

[A]	[B]	[C]	[D]	[E]	[F]
1	0.0174	0.261	0.1286	0.4927	0.2427
2	0.0348	0.522	0.2511	0.4810	0.2313
3	0.0523	0.784	0.3608	0.4625	0.2139
4	0.0697	1.0455	0.4523	0.4349	0.1892
5	0.0871	1.3065	0.522	0.4015	0.1612
6	0.1045	1.5675	0.5650	0.3622	0.1312
7	0.1218	1.827	0.5814	0.3194	0.1020
8	0.1391	2.0865	0.5699	0.2739	0.0750
9	0.1564	2.346	0.5319	0.2273	0.0516
10	0.1736	2.604	0.4708	0.1810	0.0328

TABLE 4
[α=25]

[A]	[B]	[C]	[D]	[E]	[F]
1	0.0174	0.435	0.2098	0.4824	0.2327
2	0.0348	0.87	0.3947	0.4537	0.2058
3	0.0523	1.3075	0.5220	0.4015	0.1612
4	0.0697	1.7425	0.5786	0.3325	0.1105
5	0.0871	2.177	0.5669	0.2612	0.0682
6	0.1045	2.6125	0.4671	0.1789	0.0320
7	0.1218	3.045	0.3237	0.1064	0.0113
8	0.1391	3.477	0.1498	0.0432	0.0018

TABLE 5

[$\alpha = 20$]

[A]	[B]	[C]	[D]	[E]	[F]
1	0.0174	0.348	0.172	0.4942	0.2442
2	0.0348	0.6967	0.3289	0.4720	0.2228
3	0.0523	1.046	0.452	0.4346	0.1889
4	0.0697	1.394	0.5419	0.3898	0.1519
5	0.0871	1.742	0.5792	0.3328	0.1108
6	0.1045	2.09	0.5692	0.2723	0.0741
7	0.1218	2.436	0.5131	0.2111	0.0446
8	0.1391	2.782	0.4160	0.1499	0.0224

TABLE 6

[$\alpha = 30$]

[A]	[B]	[C]	[D]	[E]	[F]
1	0.0174	0.522	0.250	0.4807	0.2311
2	0.0348	1.044	0.4523	0.4349	0.1892
3	0.0523	1.569	0.5662	0.3606	0.1300
4	0.0697	2.091	0.5682	0.2705	0.0732
5	0.0871	2.613	0.4678	0.1792	0.0321
6	0.1045	3.135	0.2890	0.0923	0.0085
7	0.1218	3.654	0.0746	0.0204	0.0042

formula agrees well in the range of scattering angles 4-8°. For our experimental set up, the range of scattering angle over which we need to obtain the experimental ratios of intensities to determine the particle sizes of unknown samples was chosen to be between 4-8°.

The apparent disagreement between experiment and theory in the range 1-3° is due to contributions of light other than scattering reaching the P.M. tube. for angles very close to the forward direction (i.e. $\theta = 0$), it is impossible to limit the contributions, other than the actual scattered light due to finite beam width of laser. Also in our experiments, the contributions due to internal reflections in the range 1-3° can not be ruled out because of the construction of the window of the P.M. tube.

[3.2.2] Sample and its mounting: The sample preparation does not involve any process. We have ready-made samples - cigarettes and sprays, which need lighting and pressing. Cigarette is lighted and kept in petridish which is then mounted on the prism table of mount for scattering. For sprays we press the atomiser keeping it in such a way that laser light intercepts the spray.

To measure the scattered intensity due to aerosols of smoke we waited for sometime till the regular flow of smoke

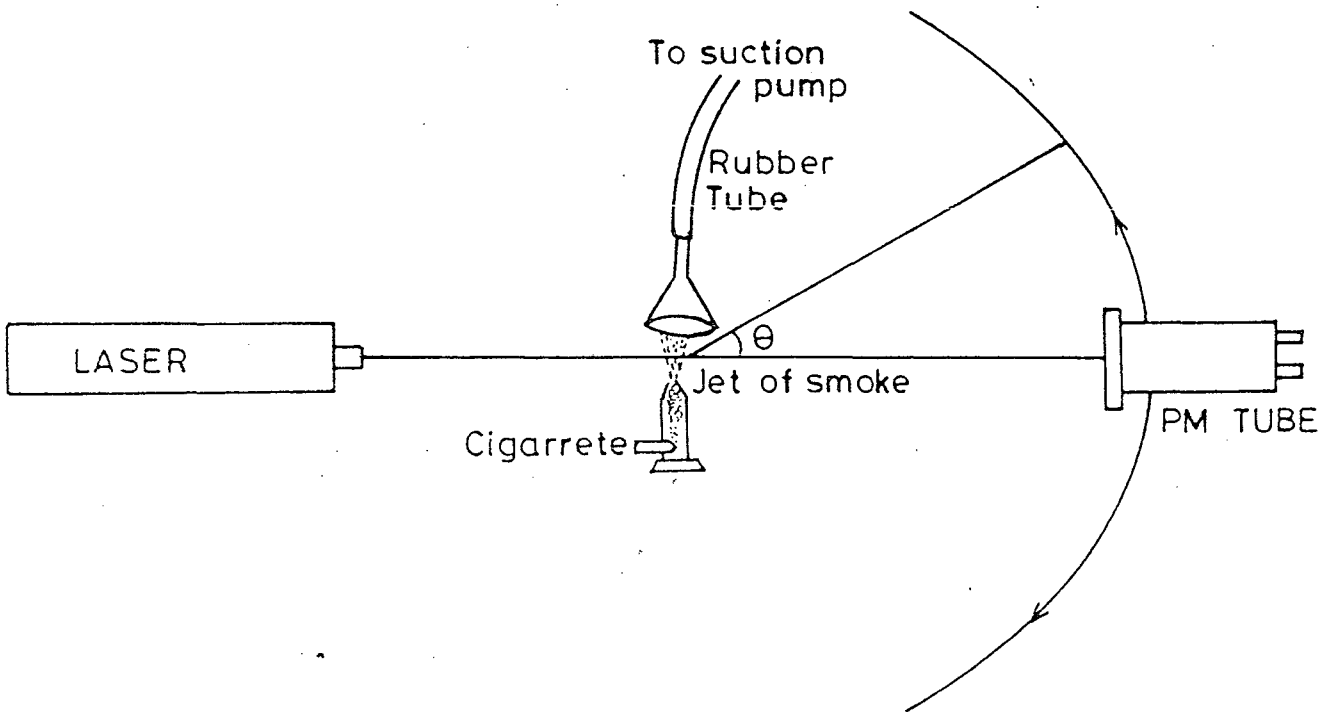

Fig. 3.4: Sketch diagram showing the movement of P.M. Tube in YZ plane, the angle of scattering denoted by 'θ' at position P_2 of the P.M. Tube.

was achieved. Then the intensity of light was measured at °C. Then the arm at which the PMT was mounted, was rotated each time by an angle of 1° and the scattered intensity was measured.

To chek the spreading of smoke and for dispersal of the particles we clamp the collecting apparatus shown in Fig. (3.7) above the petridish whose one end is fitted with suction pump. We adjust the height of the clamp so that the laser light passes through the smoke in air. Thus we get the scattering of particulates suspended in air.

[3.3] PRECAUTIONS:

To minimise the error due to vibrations the set up was kept on a heavy one-inch thick steel plate. To avoid light from other sources the set up was covered with a black wooden box with one side opening widnow. Vaccum cleaner was used to keep the experimental chamber dust free as the dust may add to the scattering. After each reading the PM tube was shifted to next angle and kept there for two to five minutes for stabilization.

Before taking the scattering measurements of smoke aerosols we checked that the flow of smoke is regular and linear.

CHAPTER IV

RESULTS AND DISCUSSION

Experimentally measured values for scattered intensity were obtained at various angular positions. Intensity as a function of scttering angle is plotted for various samples of smoke and spray. Results are shown in Figs. (4.1)-(4.5)(for smoke) and in Fig. (4.6) (for spray). Five sets of readings at every angle for each sample have been taken. Mean of the five values at a particular angle is taken as the value of scattered intensity at that angle. Bar has been put across the mean points to show the spread of radings.

In Fig.(4.1) also plotted are the theoretical values for α =15 and α = 16. Experimental points lie between these two values. Now the deviation of experimental points has been calculated with α = 15.1, 15.2,---,16. Minimum deviation is obtained for α= 15.2, so it is taken as the value for the sample, which gives particle diameter as 3.06 μm.

In Figs. (4.2) and (4.3) experimental points are shown to lie between α= 16 and α= 17. Minimum deviation is obtained for α= 16 in Fig. (4.2). The corresponding diameter is 3.22 μm. But for the Fig. (4.3), α=16.8, is

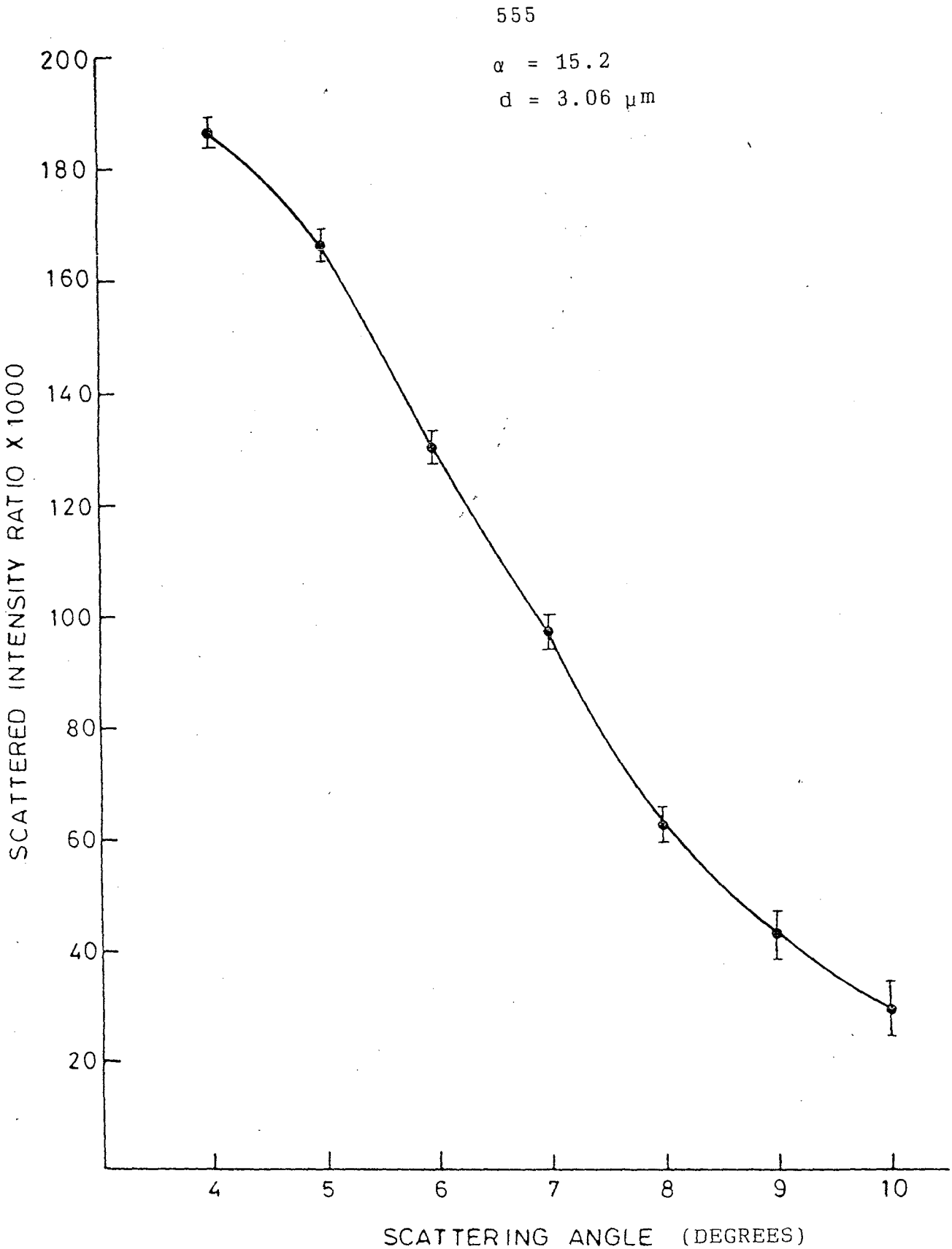

Fig. 4.1: Scattered Intensity vs. Scattering Angle for Sample 1.

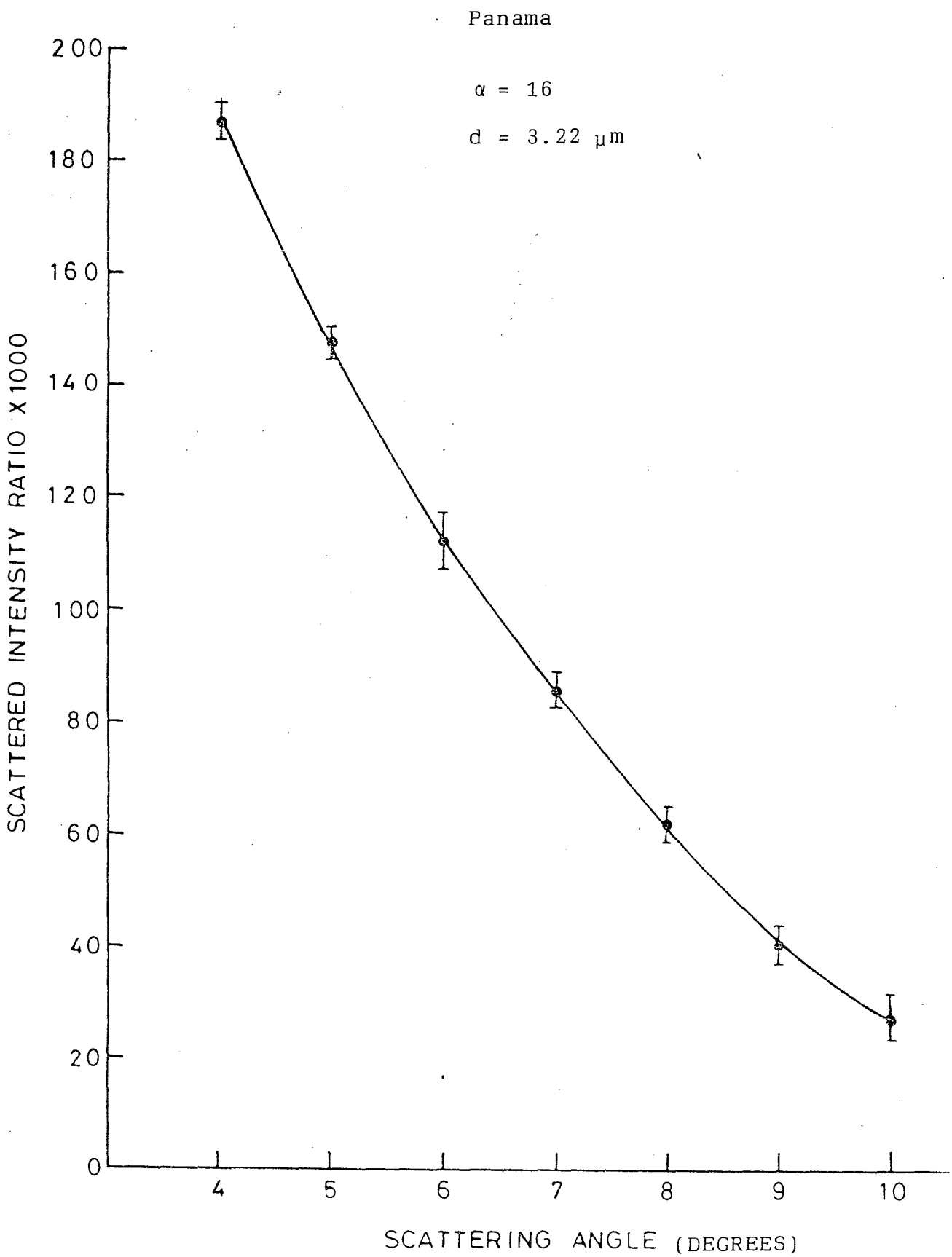

Fig. 4.2: Scattered Intensity vs. Scattering Angle for Sample 2.

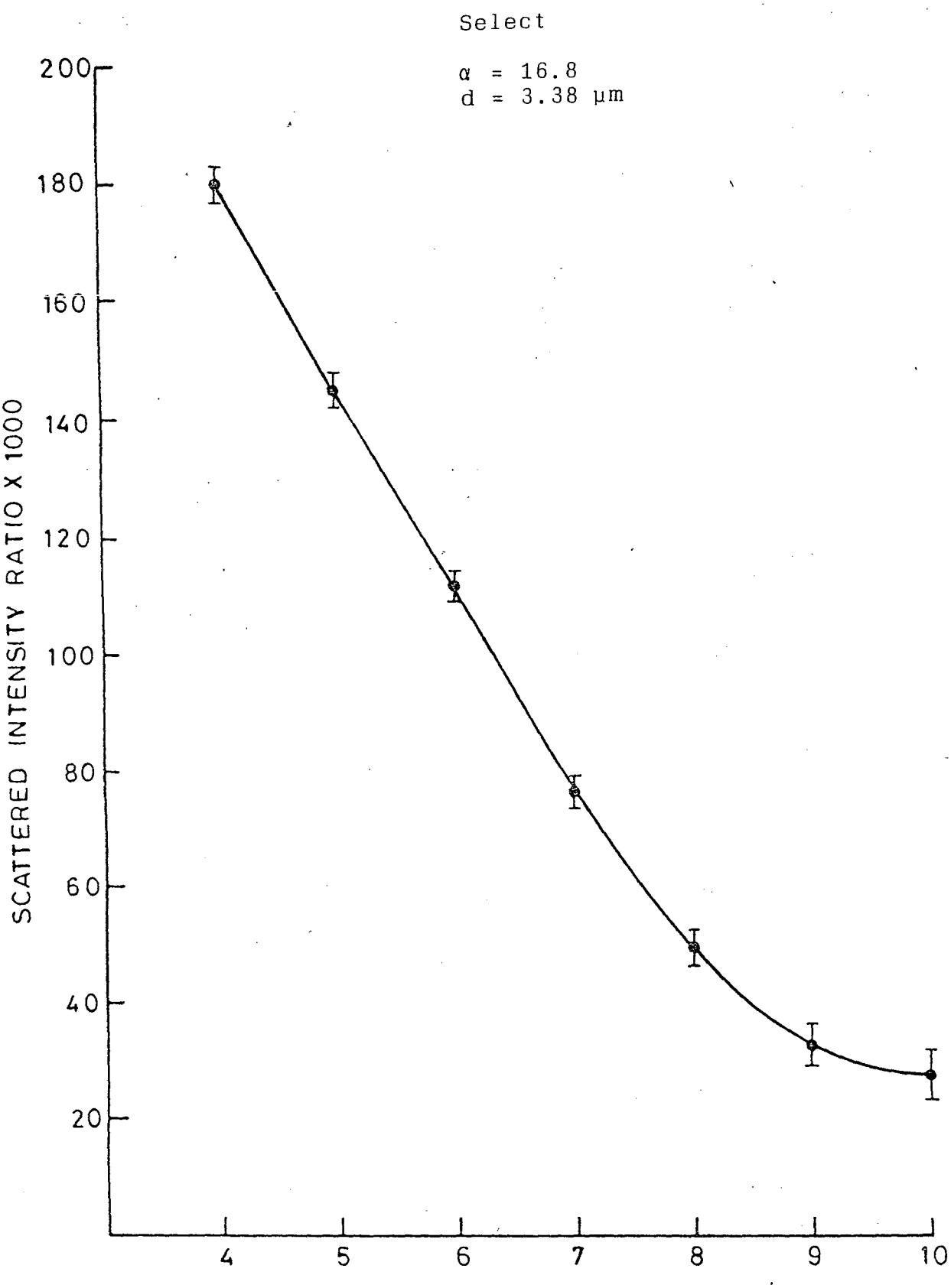

Fig. 4.3: Scattered Intensity vs. Scattering Angle for Sample 3.

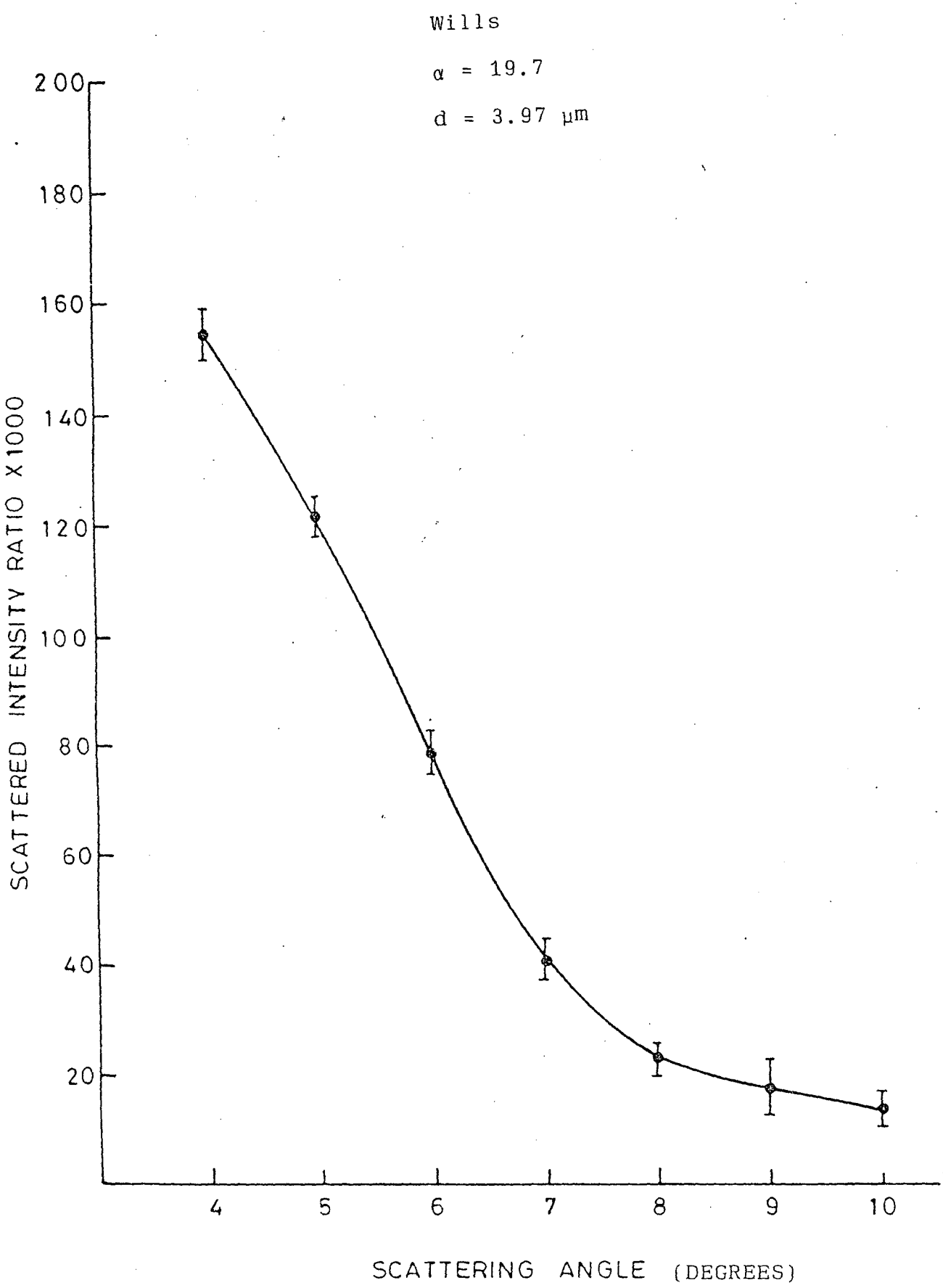

Fig. 4.4: Scattered Intensity vs. Scattering Angle for Sample 4.

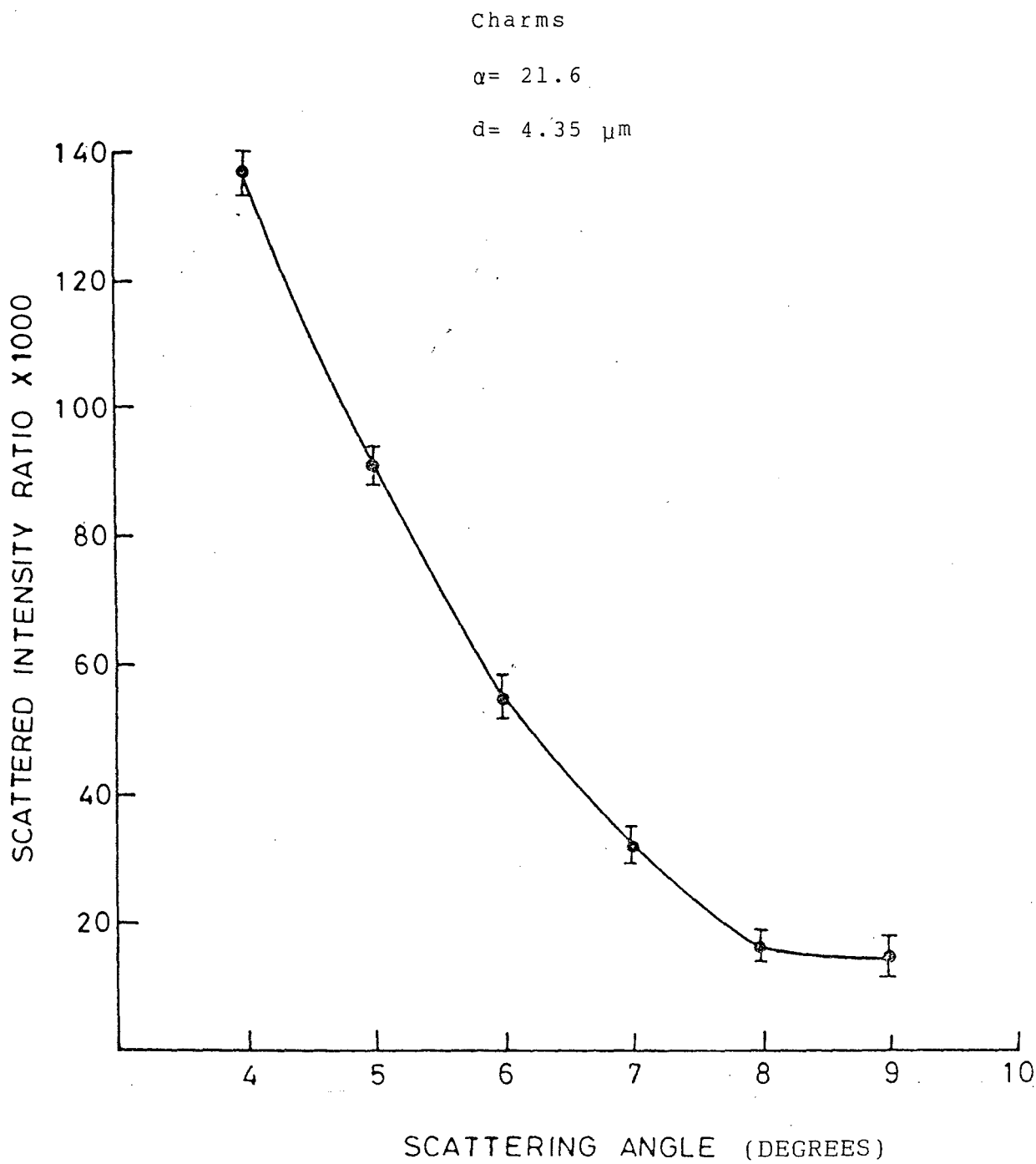

Fig. 4.5: Scattered Intensity vs. Scattering Angle for Sample 5.

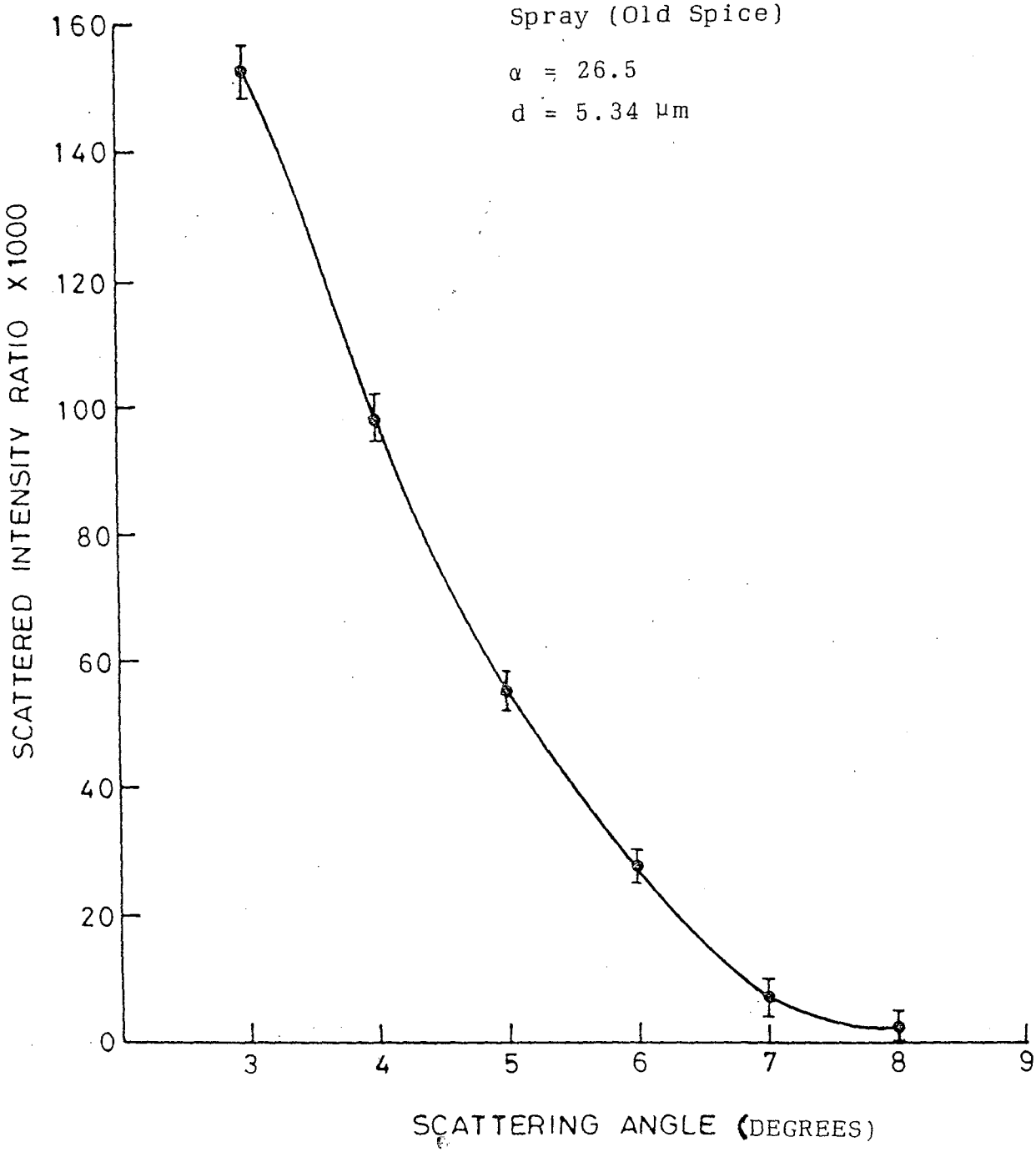

Fig. 4.6: Scattered Intensity vs. Scattering Angle for Sample 6.

the value for which the minimum deviation is obtained, so the value of diameter comes out to be 3.38 μm.

$\alpha = 19$ and $\alpha = 20$ are the theoretical values between which experimental points lie in Fig.(4.4). $\alpha = 19.7$ gives the minimum deviation with experimental points so it is taken as the value for the sample and gives the particle diameter as 3.97 μm.

Similarly, in Fig.(4.5), minimum deviation is obtained for $\alpha = 21.6$ and in Fig.(4.6) for $\alpha = 26.5$. These values of α give particle diameters as 4.35 μm and 5.43 μm. The results can be summarized as follows :

Sample		α-value	Diameter (μm)
Cigarette			
(i)	555	15.2	3.063235 ± 0.006578
(ii)	PANAMA	16.0	3.224458 ± 0.006250
(iii)	SELECT	16.8	3.385681 ± 0.005952
(iv)	WILLS	19.7	3.970114 ± 0.005076
(v)	CHARMS	21.6	4.353019 ± 0.004629
Spray			
	Old Spice	26.5	5.340509 ± 0.003773

We have obtained very high value for diameter of tobacco smoke aerosols than the standard. This can be explained as being due to two reasons. First, the

temperature of the tip of the burning cigarette remains 600-800°C. The smoke ejected at such a high temperature passes through the air at room temperature. Knowing the hydrophilic nature of tobacco smoke, it is but natural to infer the high diameter as a consequence of condensation of atmospheric vapour. Second, the Mie formula which we have used to calculate the diameter of particles is obtained on the assumption that the particles are non-interacting but for our sample, i.e. cigarette smoke, we can not say safely that the particles are independent and do not interact with other particles.

CHAPTER - V

PHOTO-CORRELATION SPECTROSCOPY

5.1 INTRODUCTION:

The term photo-correlation spectroscopy (PCS) or intensity correlation spectroscopy (ICS) designates the technique by which relevant properties of a scattering medium illustrated by a light beam are derived from the measurement of correlation function of the intensity of the scattered light.

Prior to about 1956, nearly all measurements in optics were based on mean light intensity. Although the techniques of fast pulse photoelectronics had been known for some years, it was not until the successful demonstration by Hanbury Brown and Twiss on the feasibility of photo-electric correlation measurements, that they began to be considered and applied in practice to light scattering experiments.

In the first experiments the outputs of the photodetectors were treated and processed as continuous signals, but in later experiments optical correlation was also demonstrated by the techniques of photon counting. Thus it was shown that if two photomultilpliers are

illuminated by two mutually coherent beams of light and their pulses are fed to a coincidence circuit, the rate of coincidence counting exceeds the expected rate of random pulses. It was first demonstrated by Hanbury Brown and Twiss that photoelectric correlation techniques could be applied to the determination of angular sizes of distant stellar sources, by an extension of the Michelson Stellar interferometer. Later it was pointed out that the correlation methods could be applied to the determination of very narrow spectral distributions, such as in some Brillouin scattering experiments, polarization properties of light and coherence properties of laser beams.

In the study of scattering of light by fluids, thermodynamic variables describing the system constantly fluctuate as it is fundamental to statistical mechanics, that a system of many particles never exhibit perfect uniformity. The light beams can be used to detect these fluctuations and to measure their characteristic frequencies and life times. The light source required must have high intensity and monochromaticity - such chracteristics are provided by continuous wave lasers. In order to analyze these fluctuations it is necessary to carry out either spectrum analysis or correlation analysis of the scattered light. Since these fluctuations are very slow compared to frequency of light wave, very high resolution

spectrometers are required. The resolution needed is so high that conventional optical spectroscopy fails. We have to use correlation techniques as it is well known, the optical spectrometers can not resolve spectrum components narrower than 10MHz. However, the thermal fluctuations of dieletric constant of the medium can produce spectrum lines with width as narrow as 10Hz.

The spectral information of the scattered light can be obtained by optical mixing spectroscopy but the digital intensity correlation techniques have the advantage of being faster and giving much better statistical accuracy.

In the last few years ICS has found many areas of applications in physics, chemistry, biology, and engineering. Its understanding requires an acquaintance with the statistics of light fields, theories of light scattering, and some knowledge of optical and electronic instrumentation. We shall discuss here a fews important points, with the aim of making clear the basic principles of ICS.

(5.2) THEORY

(5.2.1) Properties of Corrlation Functions

The statistical properties of any random process (such as an optical field) can be characterized by joint

probability distributions or (and) correlation functions of any order. In practical cases relevant information on optical fields is obtained by measuring only the lowest order correlation functions $G^{(1)}$ and $G^{(2)}$ defined as follows:

$$G^{(1)}\left(\vec{r}_1,\vec{r}_2,\tau\right) = \langle E^{*}(\vec{r}_1,t)\, E(\vec{r}_2,t+\tau)\rangle \qquad (5.1)$$

and

$$G^{(2)}\left(\vec{r}_1,\vec{r}_2,\tau\right) = \langle I(\vec{r}_1,t)\, I(\vec{r}_2,t+\tau)\rangle \qquad (5.2)$$

Where E and $I = |E|^2$ are respectively the electric field and the intensity of the optical beam.

Quite generally it can be said that the spatial properties of correlation functions reflect merely the geometry of the source (the scattering volume in a light scattering experiment). We are here more interested in time dependence of $G^{(1)}$ and $G^{(2)}$ which contains information about the dynamics of source fluctuations. We put therefore $\vec{r}_1 = \vec{r}_2$. Furthermore, we consider only stationary fields, so that $G^{(1)}$ and $G^{(2)}$ depend only on the time delay τ

Properties of $G^{(1)}(\tau)$

$$G^{(1)}(0) = \langle I\rangle;\quad |G^{(1)}(\tau)| \leq G^{(1)}(0);\quad \lim_{\tau\to\infty} G^{(1)}(\tau) = 0$$

Properties of $G^{(2)}(\tau)$

$$G^{(2)}(0) = \langle I^2\rangle;\quad \lim_{\tau\to\infty} G^{(2)}(\tau) = \langle I\rangle^2;$$

$$|G^{(2)}(\tau) - \langle I\rangle^2| \leq G^{(2)}(0) - \langle I\rangle^2$$

We recall also the definition of the optical spectrum $S^{(1)}$ ( )

$$S^{(1)}(\omega) = \int G^{(1)}(\tau)\, e^{i\omega\tau}\, d\tau \qquad (5.3)$$

If $S^{(1)}(\omega)$ is a symmetric function with respect to the central fequency ω_o, and we write the field as

$$E(t) = E_o(t)e^{-i[\omega_o t+\Psi(t)]} \quad (E_o(t) \text{ real})$$

the correlation functions can be expressed as:

$$G^{(1)}(\tau) = \langle 1\rangle\, e^{i\omega_o\tau}\, f(\tau) \qquad (5.4)$$

$$G^{(2)}(\tau) = \langle I\rangle^2\, (1+g(\tau)) \qquad (5.5)$$

Where $f(\tau)$ and $g(\tau)$ are real.

The following relation holds for gaussian fields

$$g(\tau) = f^2(\tau) \qquad (5.6)$$

It should be noted that knowledge of $G^{(2)}$ does not give completely $G^{(1)}$ even for gaussian fields. The information about the central frequency ω_o is lost.

(5.2.2) Light Scattering: Generalities:

A schematic light scattering experiment is sketched in Fig. 5.1. A monochromatic plane wave, linearly polarized is incident upon a perfectly uniform transparent medium.

An optical detector in position P reveals the presence of a nonzero light intensity, generally weak, propagating in

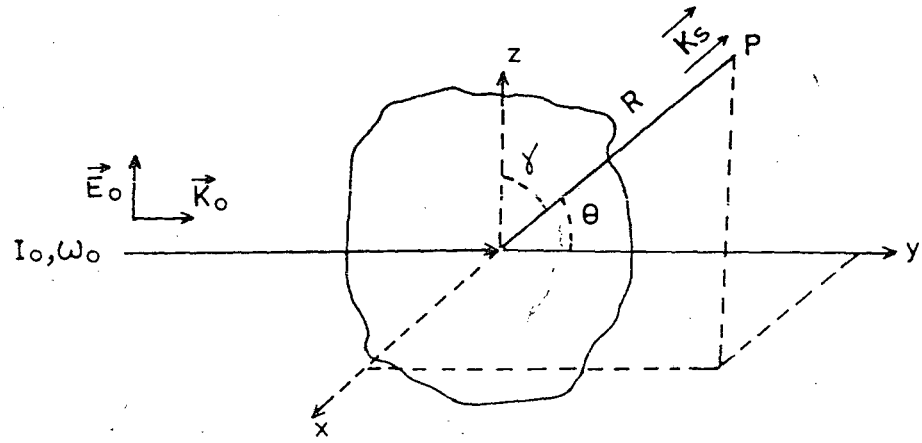

Fig. 5.1: Schematic light scattering experiment

directions other than that of reflected and refracted beam. This is what is called scattered light.

In Fig. 5.1, the incident beam propagates along the Y-axis and is linearly polarized along the Z-axis; ω_o and I_o are respectively its angular frequency and its intensity. The scattered light is observed at the point P having polar coordinates (R, θ, γ). θ is the angle between $\vec{K}_o$ and $\vec{K}_s$. The effective volume V which contributes to the scattered field collected at P does not include the entire sample, but is rather defined by cross-section of incident beam and the detection optics. The distance R is taken to be much larger than the linear size of the scattering volume V.

The physical origin of the scattering process can be understood in the following way. The illuminated medium interacts with the incident electric field at optical frequency through an electric polarizability per unit volume $\chi(\vec{r},t)$. For the sake of simplicity the medium is assumed to be optically isotropic (χ is a scaler quantity) and linear (χ is independent of amplitude of the incident field). The field radiated by each volume element follows the well-known dipole radiation pattern. The field collected by a detector placed in the position P is the sum, with appropriate phases of the contributions from each volume element. It is easy

to show that if $\chi(\vec{r},t)$ is independent of $\vec{r}$, we get destructive interference in any direction, apart from that of the refracted beam. If, however, χ is a fluctuating function of $\vec{r}$, all the elementary contributions to the scattered field will not completely cancel out, and we do expect a nonzero scattered intensity.

The polarizability χ can always be written as

$$\chi(\vec{r},t) = \langle\chi\rangle + \delta\chi(\vec{r},t)$$

where $\langle\chi\rangle$ is the average part, independent of $\vec{r}$ and t for a homogeneous medium in stationary conditions, and $\delta\chi(r,t)$ is the fluctuating part, which has zero average. From the intuitive considerations given above, it is clear that scattering is produced by $\delta\chi(\vec{r},t)$.

The theoretical computation gives the following expression for the scattered field $E_s(\vec{R},t)$:

$$E_s(\vec{R},t) = \frac{1}{\langle\varepsilon\rangle}\,\vec{K}_s.(\vec{K}_s.\vec{E}_o)\,\frac{Ve^{i(\vec{K}_s\vec{R} - \omega_o t)}}{4\pi R}\,\delta\varepsilon(K,t)$$

where $\varepsilon = 1 + \chi$ is the relative dielectric constant of the medium, V is the volume, $\vec{K}_s$ is the wave vector of the scattered field, and $\delta\varepsilon(\vec{K},t)$ is defined by the Fourier transformation :

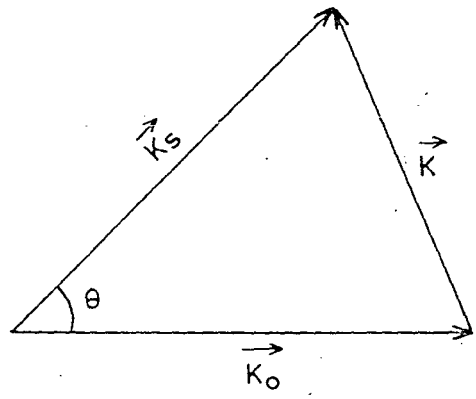

Fig. 5.2: Triangle of wave vectors. If $k_s \simeq k_o$, the triangle is practically isoceles.

$$\delta\varepsilon\ (\vec{K},t) = \frac{1}{V} \int_{v} \delta\varepsilon(\vec{r},t)\ e^{-i\vec{K}.\vec{r}}\ d^3r \qquad (5.8)$$

The vector $\vec{K}$, as shown in Fig.[5.2], is defined by:

$$\vec{K} = \vec{K}_s - \vec{K}_o \qquad (5.9)$$

Equations (5.7 - 5.9) indicate that of all the Fourier components of the fluctuation in dielectric constant only that particular component whose wave vector is the difference between the wave vectors of the scattered and the incident light is responsible for scattering in the direction of observation.

Equation (5.7) has been derived by using a perturbation approach which takes $\delta\chi\ (\vec{r},\ t)$ to be small compared to $\langle \chi \rangle$ and which assumes the attenuation of the incident field to be negligible over the whole length of the scattering volume. Multiple scattering effects are, therefore, assumed to be very weak.

The scattered field $E_s\ (\vec{R},t)$ is a random function of position and time with a zero average. The time dependent fluctuations of E_s exactly mirror the fluctuations in dielectric constant of wave vector $\vec{K}$. Fluctuations in dielectric constant are generally much slower than an

optical period, that is, the energy associated with an elementary excitation in the medium is much smaller than the energy of incident optical photon. As a consequence, the energy conservation theorem tells us that the energy of the scattered photon is practically the same as that of the incident one. By putting $|\vec{K}_s| = |\vec{K}_o| = K_o$, the momentum conservation relation (5.9) gives $K = 2K_o \sin\theta/2 = \frac{4\pi n}{\lambda}\sin\theta/2$ where n is the refractive index of the medium and θ is the angle between $\vec{K}_o$ and $\vec{K}_s$.

The space dependent fluctuations of $\vec{E}_s$ depend only, in usual cases on the geometry of the experiment. Indeed, if we compare $\vec{E}_s(\vec{R},t)$ with $\vec{E}_s(\vec{R}+\delta\vec{R},t)$, where $\delta\vec{R}$ is a displacement on the sphere of radius R centered at the origin of the coordinate system, we find that both amplitude and phase of $\vec{E}_s$ are different since the relative phases of the scattered fields from each volume element change by moving from $\vec{R}$ to $\vec{R}+\delta\vec{R}$. The coherence area A_c of the scattered field is qualitatively defined as the area (on the sphere of radius R) over which the scattered field is appreciably uniform in amplitude and phase. A more precise definition would imply the use of spatial correlation function for the scattered field. The coherence area is given by:

$$A_c \quad \frac{\lambda^2 R^2}{A_s(\theta, \gamma)} \qquad (5.10)$$

where $A_s(\theta, \gamma)$ is the area intersected on the scattering volume by a plane perpendicular to R and passing through the center of the scattering volume. It is evident from this definition that A_c depends upon the observation direction, that is the angles θ and γ. The ratio λ^2/A_s is called the coherence solid angle. Equation (5.10) can be interpreted as an extension of the well-known result of the one dimensional grating of size a, which gives a diffraction angle λ/a and, therefore, a spot size $\lambda R/a$ at a distance R.

The scattered field $\vec{E}_s(\vec{R},t)$ at a given point is a random function of time. A complete characterization of it is given by the set of correlation functions:

$$G_m(t_1,\ldots,t_{2m}) = \langle E_s^*(t_1)\ldots E_s^*(t_m)E_s(t_{m+1}) \ldots E_s(t_{2m})\rangle$$

where m runs from 1 to infinity. By using equation (5.7), a one to one correspondence between the correlation functions of the field and those of the dielectric constant can be established.

(5.2.3) Light Scattering: Macromolecular solutions

In a macroscopic system in thermal equilibrium at a temperature T, local fluctuations of the dielectric constant

are caused by fluctuations in the thermodynamic parameters describing the state of the system. For instance, in a pure fluid the value of $\delta\varepsilon(\vec{r},t)$ is mainly determined by local density fluctuations. We will discuss now a specific example, that is light scattering from a suspension of noninteracting macromolecules, small compared with the wavelength of light. For such a system, containing N_s macromolecules in the scattering volume

$$\delta\varepsilon(\vec{r},t) = \Delta\varepsilon_r \sum_{i=1}^{N_s} \delta\,(r - r_i(t)] \qquad (5.11)$$

where $\Delta\varepsilon_r$ is the difference in relative dielectric constant between a macromolecule and solvent, and $r_i(t)$ is the position of macromolecule $\vec{i}$ at time t. Equation (5.7) becomes (taking $\vec{K}_s \quad \vec{E}_o$)

$$\vec{E}_s(\vec{R},t) = \frac{E_o K_o^2}{4\pi\langle\varepsilon\rangle R} e^{i(\vec{K}_s\vec{R} - \omega_o t)} \Delta\varepsilon_r \sum_{i=1}^{N_s} \exp\,[i\vec{K}.\vec{r}_i(t)] \qquad (5.12)$$

This result can also be obtained directly by regarding each macromolecule as an elementary dipole radiator. The electric field correlation function is given by

$$G^{(1)}(\tau) = \frac{|(E_o^2)|K_o^4\Delta\varepsilon_r^2}{16\pi^2\langle\varepsilon\rangle^2 R^2} e^{i\omega_o\tau} \sum\sum \langle\exp\{iK[\vec{r}_i(t)-\vec{r}_j(t+\tau)]\}\rangle \qquad (5.13)$$

For independent scatters, the position of particle i will at all times be uncorrelated with the position of particle j.

Thus only the terms for i = j will contribute to the double sum of Eq.(5.13). For random walk diffusion under the influence of Brownian motion it is easy to show that

$$G^{(1)}(\tau) = \langle I_s \rangle \exp(i \omega_o \tau) \exp(-DK^2\tau) \qquad (5.14)$$

where $\langle I_s \rangle$ is the average scattered intensity and D is the translational diffusion coefficient of the macromolecule. An intuitive justification of this result comes from the fact that $(DK^2)^{-1}$ is roughly the time taken by a macromolecule to diffuse a distance 1/K. If N_s is not too small, the scattered field, being the superposition of many statistically independent contributions, is gaussian. The intensity correlation function is therefore immediately derived from Eqs.(5.14) and (5.6) and reads

$$G^{(2)}(\tau) = G^{(1)}(o)^2 + |G^{(1)}(\tau)|^2$$

$$= \langle I_s \rangle^2 [1+\exp(-2DK^2\tau)] \qquad (5.15)$$

(5.3) Particle size determination

We define,

$$\tau_c = (2DK^2)^{-1} \qquad (5.16)$$

as the characteristic relaxation time for the decay of the correlation function, which can be obtained by photon

correlators. Thus, getting τ_c experimentally, D can be found out putting the value of K which is known.

Now, D the mutual diffusion coefficient, in the limit of infinite dilution is given by the well known Einstein-Stoke's relation

$$D_o = \frac{K_B T}{6 \pi \eta r} \qquad (5.17)$$

where D_o = Diffusion coefficient at infinite dilution

K_B = Boltzmann constant

T = Absolute temperature

η = Viscosity of the solvent.

r = Radius of the particle.

Therefore,

$$r = \frac{K_B T}{6 \pi \eta D_o} \qquad (5.18)$$

5.4 Photon Correlators

There are numerous techniques for determining the intensity correlation function of the light beam. Here we shall describe two of them: the first, the so called clipping technique which is quite simple but usually valid for thermal light and the second which involves use of time

to amplitude converter is more general and is valid for all kinds of light beams.

5.4.1 Clipping technique

The most convenient approach is to count the number of detections occurring during continuous sample times of duration T chosen to be short compared with the correlation times under study. The normalized autocorrelation function of photon counting fluctuations in this time can be written as

$$R(\tau) = \frac{\langle n_T(t)\, n_T(t+\tau)\rangle}{\langle n_T(t)\rangle^2} \qquad (5.19)$$

where $n_T(t)$ is the number of detections occurring during a sample time t and t+T.

There is however, a difficulty in taking the product $n_T(t)\ n_T(t+\tau)$ associated with the fact that multiplication of numbers greater than one is time consuming and therefore limits the ultimate speed of such a correlator. To overcome this a clip level K is selected so that the clipped signal $n_K(t)$ follows the conditions

$$n_K(t) = 1 \quad \text{if } n(t) > K$$

$$= 0 \quad \text{if } n(t) \leq K$$

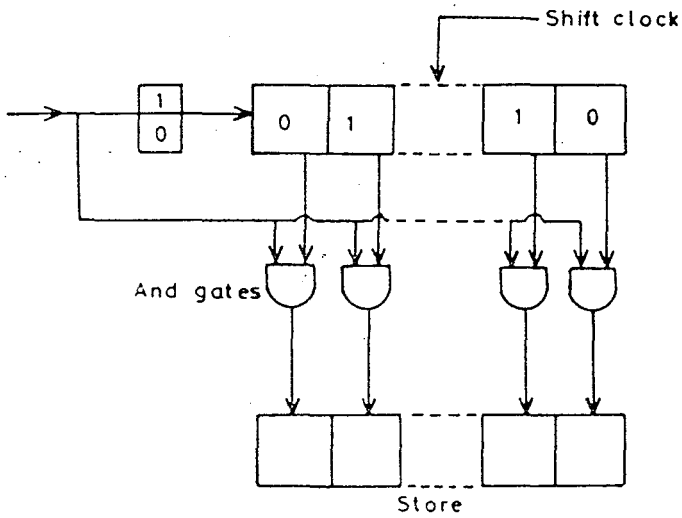

Fig. 5.3: A block diagram of the clipping correlator.

By using the one bit quantized clipped signal only in delay channel, the complexity of the multiplication is reduced to a gating function as shown in Fig.[5.3]. Since multiplication of n(t) by $n_K(t+\tau)$ is equivalent to gating n(o) by $n_K(\tau)$. This reduction in complexity leads to considerable increase in operating speed. The single clipped auto correlation function $R_K(\tau)$ for delay τ is given by

$$R_K(\tau) = \frac{\langle n_K(\tau)\, n(o)\rangle}{\langle n_K(o)\rangle\langle n(o)\rangle} \qquad (5.20)$$

from where we can have

$$R_K(\tau) = 1 + f\,\frac{1+K}{1+\langle n_T\rangle}\,|R_E(\tau)|^2$$

where $R_E(\tau)$ is the normalized amplitude correlation function and f is the correlation factor affecting the ratio of the spectral term to the background. A commercial correlator using this technique is now available.

5.4.2 Use of time to amplitude converter

Time resolved photoelectric correlation measurements are most easily carried out with the help of a combination of a time to amplitude converter and pulse height analyser as shown in Fig.[5.4]. The light beam to be studied is split into two parts by partially silvered mirrors and beams

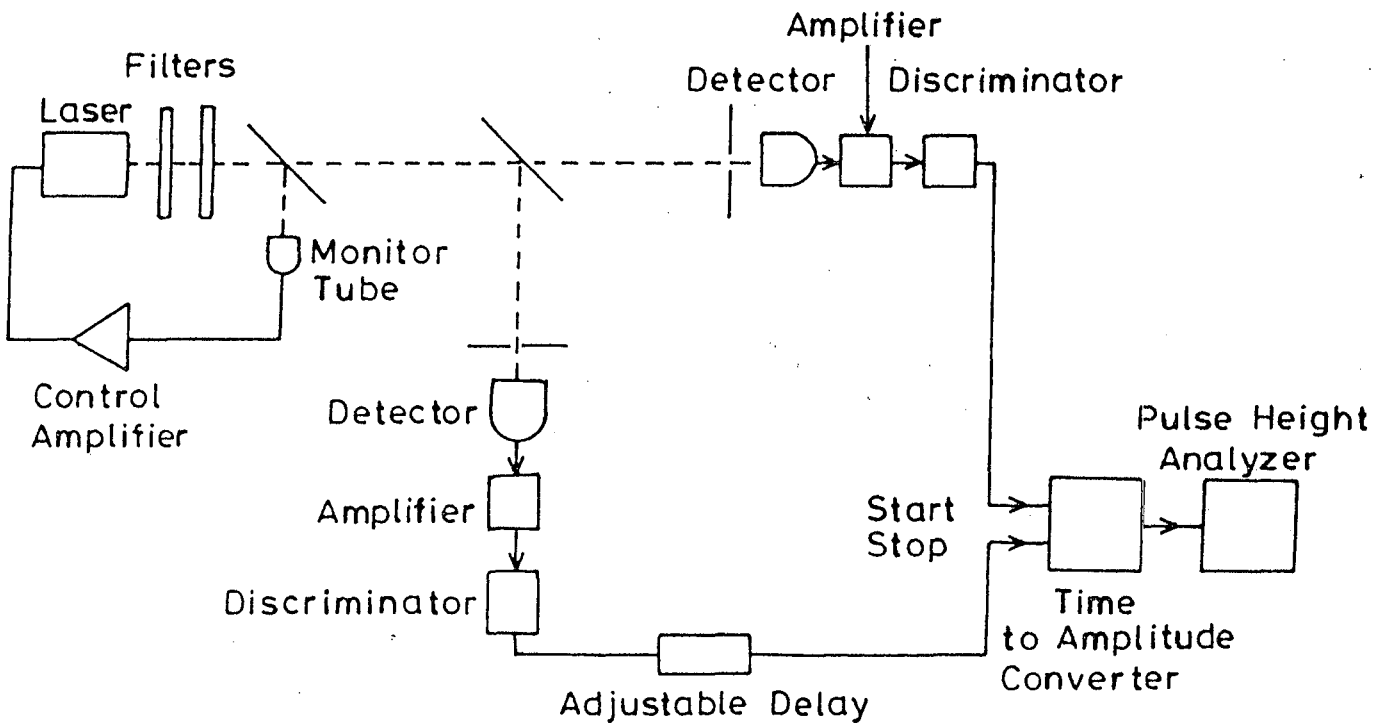

Fig. 5.4: Outline of a set up for intensity correlation measurement using time-to-amplitude converter.

fall on two separate phototubes. The photoelectric pulses from the two detectors after suitable amplification and shaping are fed to the start and inputs of time to amplitude convertor (TAC). This is an electronic device in which the start pulse initiates a ramp wave form which is cut off when the stop pulse is received. The output from TAC is therefore a pulse whose amplitude is proportional to the time interval between the two input pulses, and the various output pulses are sorted, into appropriate channels by a multichannel pulse height analyzer. The distribution of pulse heights registered by the analyzer is therefore a measure of the distribution of time intervals between photoelectric pulses.

Nevertheless, this probability distribution can not be immediately identified with the expression for $G^{(2)}(\tau)$. In order that an event corresponding to the time interval t to $t+\tau$ shall be registered by the TAC, it is necessary not only that a start pulse is received at time t and a stop pulse at time $t+\tau$, but also that no other stop pulse appears in between. This makes the extraction of intensity correlation function little complicated by the fact that for making straight forward measurement of $G^{(2)}(\tau)$ one has to keep the counting rates low, thus affecting the statistical accuracy of the measurement. A considerable modification of this technique using elaborate electronics exists.

Now-a-days, simple, cheap microprocessor-controlled photon correlators based on the principle of measuring the arrival times of photo electrons are also available. These are equally applicable to guassian as well as non-guassian radiation.

CHAPTER VI

CONCLUSION

First, we verified approximation formula for forward and small angle scattering obtained from Mie theory of scattering which assumes particles to be spherical and noninteracting. For verification, we have used known sizes of hydrosols of Ferric hydroxide which is a hydrophilic sol and is a good example of idealized situation of separated particles in a homogeneous medium. Hydrosols of sizes 2.3 and 5 microns were obtained using sedimentation technique. The variation of the experimentally observed scattered intensity as a function of θ agreed well with that obtained from theory.

The verification of Mie theory confirms the suitability of our experimental system for scattering experiments. Experiments were done on smoke and spray aerosol samples. Five sets of readings were taken for each sample. An experimental curve for scattering intensity ratio i.e. $i(\theta)/i(0)$ vs. scattering angle is obtained with mean experimental points. Comparison of this curve with the theoretical curve gives the size parameter and consequently the diameter of aerosol particles. The typical sizes for smoke and spray aerosols were found to be 3.06 μm, 3.22 μm, 3.38 μm, 3.97 μm, 4.35 μm and 5.34 μm.

The diameter of the smoke particles are found to be much greater than those reported in standard tables. But the consistency of our experiment with theory indicates that there are other reasons than the nonapplicability of Mie scattering theory to smoke particles. the probable reasons for this discrepancy may be condensation of atmospheric vapour, nonspherical and interacting nature of particles.

Finally we have reviewed the photon correlator technique in which the temporal relation of scattered photons is used to determine the properties of the scattering material. From the correlation curve, the characteristic decay time can be inferred which can be used to determine particle size. It is a very sensitive and accurate technique for determining the particle size. Experiments based on the applications of this technique for the particle size determination are planned for future work.

APPENDIX A

Health Effects

The hazards of inhaling particulate matter, greatly depend on the concentration of deposits at specific sites or regions of the lung, their retention time and toxicity. Although fine particles are chemically diverse, their penetration and point of ultimate deposition are mostly determined by their physical size. The "aerodynamic diameter" (diameter equivalent to that of a spherical particle that settles at the same rate as the particle considered) which is dependent on particle size and diameter, largely determines the fate of inhaled aerosols.

The first size related factor in the deposition of particles is the penetration into the respiratory system (Fig. 1). Unlike large particles, fine particulates easily reach the lower lung. It is well known that all but a small fraction of particles larger than 10 micrometers in aerodynamic diameter are trapped in the nasal passages and prevented from entering the lung. But if the aerodynamic diameter is less than 5 micrometers, a particle can penetrate deeply into the respiratory system (Lippman, 1977; Marrow, 1973; Yeh et al., 1976).

Fine particles easily penetrate to all parts of the respiratory system and get deposited in each of its parts.

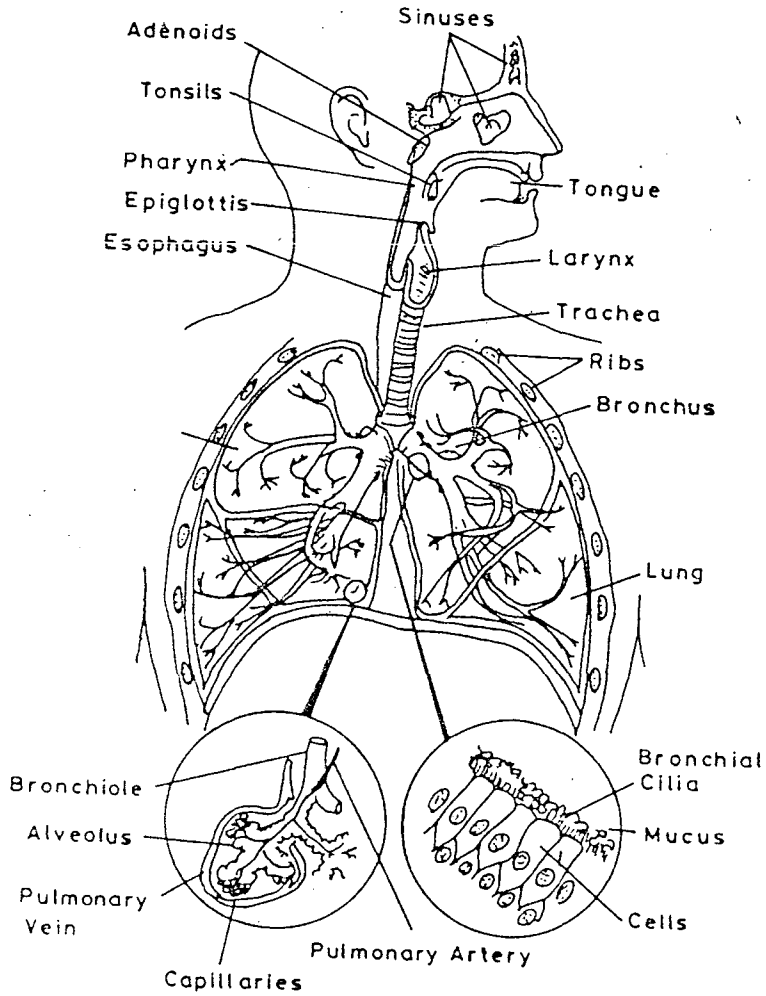

Fig. 1. The Respiratory System

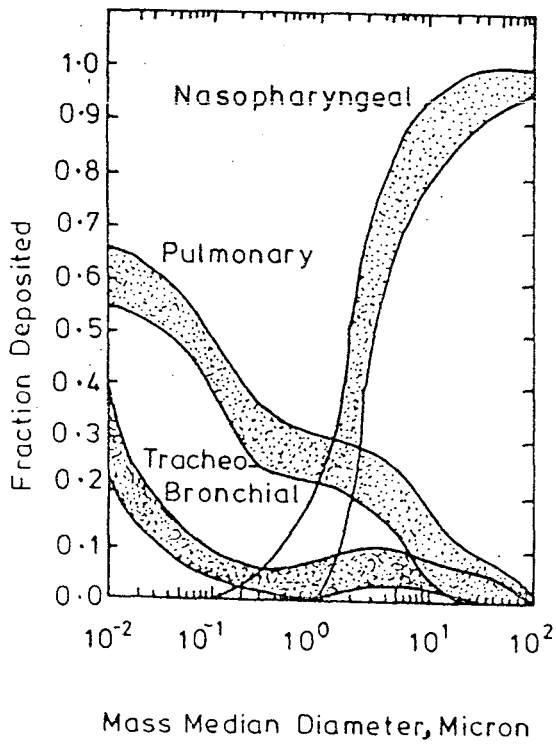

Fig. 2: Predictions of Deposition of Paticles in the Lung (ICRP)

Fig. 2 shows the theoretical deposition efficiencies of particles in three respiratory compartments. Particles greater than 10 μm are almost all deposited in the nasopharyngeal system with only a small fraction retained in the pulmonary region. Maximum efficiency of deposition is seen in the alveoli or pulmonary region for particles smaller than 2 micrometers (Wilson and Mer, 1948; Palm, 1965; Committee on the Inter-national Radiological Protection, 1966). Retention time, that is, the interval of time that particles remain in the lung, differs by site of deposition.

Removal of deposited particles from the pulmonary region may vary widely according to the solubility and reactivity of the particulate material. For example, soluble particles are believed to enter the pulmonary blood within minutes, whereas insoluble particles are removed at a very slow rate with clearence time a month or more.

Comparison of the clearance rate of insoluble particles from the various compartments of the lung showed striking differences. Exposure of experimental animals to insoluble dye particles showed clearance of particles of 2 micrometers to be markedly slower than for those of 6 micrometers. The larger particles were cleared six times as

rapidly as the small particulaes of 2 micrometers. The toxicity of particles retained in the lungs varies with chemical composition. However, a particle, which is chemically inert, by its physical presence in the lung it may interfere with and retard the clearance of toxic material present in other deposited particles. It may act as a carrier particle for gaseous pollutants and can therefore, produce synergistic effects harmful to human health. Carbon or 'soot', for example, is a common particulate pollutant with demonstrated absorbent qualities.

Table given below summarizes possible biological responses following deposition of particles in respiratory tract (Shannon et al., 1974; Corn, 1972).

Possible Effects Produced by Inhaled Particulate Matter After Deposition in Respiratory Tract Compartments

Compartment in which deposition occurs	Soluble particle	Insoluble particle
Nasopharyngeal	1. Damage to mucosa and paralysis of cilia 2. Allergic Response	1. Transferred to gastrointenstinal tract 2. Removed with sputum 3. Allergic Response
tracheobronchial	1. Reflex bronchoconstriction 2. Allergic response 3. Damage to mucosa and paralysis of cilia 4. Succeptibility to infection 5. Potentiation if gas (SO_2, NO_2,O_3, etc.) exposure present.	1. Short term clearance to gastrointenstinal tract 2. Removed with sputum
Pulmonary	1. Damage to alveolar epithelium 2. Peripheral respiratory unit constriction 3. Potentiation if gas (SO_2, NO_2,O_3, etc.) exposure present May lead to release of proteolytic enzymes and eventual emphysema with alevolar destruction.	Long term retention: 1. React with tissue to cause local effects 2. Remain in tissue (inert) 3. Transported to lymph nodes. Short-term retention: Phagocytized and transported to terminal bronchioles with subsequent clearance from tracheobronchial compartment.

REFERENCES

1. Ackerson, B.J., J. Chem. Phys. 64, 242, 1976.

2. Ackerson, B.J., J. Chem. Phys. 69, 684, 1978.

3. Bateman, J., Weneck, E.J. and Eshler, D.C. J. Coll. Sci. 14(3), 308, 1959.

4. Berry, C.R., J.O.S.A., 52(8), 885, 1962.

5. Bohidar, H., Kulkarni, S., Prasad, S. and Chopra, S., J. Phys. E. Sci. Instrum., 13, 1980.

6. Bohider, H. and Chopra, S., Optial and Quantum Electronics, 13, 1981.

7. Bridge, D.P. and Corn, M., Envir. Res., 5, 1972.

8. Briggs, J. and Nicoli, D.F., J. Chem. Phys., 72, 6024, 1980.

9. Cabannes, J., "La diffusion moleculaire de lumiere", Paris, 1929.

10. Chin, J.H., Sliepcevich, C.M. and Tribus, M., J. Chem. Phys., 59(5), 841, 1955.

11. Chopra, S. and Mandel, L., Rev. Sci. Instrum. 43, 1972.

12. Chopra, S., Physics News, 9(2), 1978.

13. Chu, B., Xu, R. and Di Napoli, A. J. Coll. Inter. Sci. 116, 182, 1987.

14. Chu, C.M. and Churchill, S.W., J.O.S.A., 45(11), 958, 1955.

15. Chu, C.M. and Churchill, S.W., J. Phys. Chem., 59(9), 855, 1955.

16. Churchill, S.W., Clark, I.G. and Sliepcevich, C.M., Disc. Farad. Soc. 30, 192, 1960.

17. Chylek, P., J. Opt. Soc., 67, 1348, 1977.

18. Clarke, C.G., Chu, C.M. and Churchill, S.W., J.O.S.A., 47, 81, 1957.

19. Cohen, A., Derr, V.E., McNice, G.T. and Cupp, R.E., Applied Optics, 12, 779, 1973.

20. Cohen, D., Arai, S.F. and Brain, J.D., Science, 204, 1979.

21. Cowen, S.J., Ensor, D.S. and Sparks, L.E., Atom. Env., 15(12), 2531, 1981

22. Cummins, H.Z. and Pike, E.R., eds., Photon Correlation and Light Beating Spectroscopy, Plenum, New York, 1974.

23. Cummins, H.Z. and Pike, E.R., eds., Photoncorrelation spectroscopy and velocimetry, Plenum, N.Y., 1977.

24. Cummins, P.G. and Staples, E.J., J. Phys. E. Sci. Instrum., 14, 1981.

25. Curcio, J.A., J.O.S.A., 51(5), 548-551, 1961.

26. Davis, C.N., "Recent Advances in Aerosol Research", Pergamon Press, 1964.

27. Debye, P., Ann. Physik, 30(4), 57, 1909.

28. Deirmendjian, D., Clasen, R. and Viezee, W., J.O.S.A., 51(6), 620, 1961.

29. Degiorgio, V., Winter College on atomic and molecular physics, International Centre for Theoretical Physics, Trieste (Italy), 1977.

30. Dicke, R.H., Phys. Rev., 93(1), 1954.

31. Ellison, J.M., Proc. Phys. Soc. B., 70, 102, 1957.

32. Ellison, J.M. and Peetz, C.V., Proc. Phys. Soc., 74, 105, 1959.

33. Friedlander, S.K., "Smoke, Dust and Haze", Wiley, N.Y., 1977.

34. Fuchs, N.A., "The mechanics of Aerosols", Pergamon Press, 1964.

35. Fuchs, N.A., Atm. Env., 9, 697, 1975.

36. Geise, R.H., Z. Nururfosch, 149(12), 1085, 1959.

37. Gucker, F.T. and Rowell, R.L., Disc. Farad. Soc., 30, 185, 1960.

38. Gucker, F.T. and Egan, J.J., J. Coll. Sci., 61(1), 68-84, 1961.

39. Gulari, Esin, Gulari Erdogan, Tsunashime, Y. and Chu, B., J. Chem. Phys., 70, 3965, 1979.

40. Gumprecht, R.O. and Sliepcevich, C.M., Tables of Light Scattering functions for spherical particles (Univ. of Michigan, Ann Arbour), 1951.

41. Hanbury Brown, R. and Twiss, R.Q., Nature, 176 (4548), 1956.

42. Hanbury Brown, R. and Twiss, R.Q., Nature, 177 (4497), 1956.

43. Heller, W. and Tabibian, R., J. Phy. Chem. 66(10), 2059, 1962.

44. Hinds, W.C., Aerosol Technology: Properties, behaviour and measurement of air borne particles, Wiley Interscience, N.Y., 1982.

45. Hodkinson, J.R. and Greenleaves, I., J.O.S.A., 5(3), 577, 1963.

46. Hodkinson, J.R., Appl. Opt., 5, 839, 1966.

47. Holland, A. and Gauge, G., Appl. Opt., 9, 1113, 1970.

48. Hoyte, J.M., Poly, Mater. Scien. Eng., 53, 156, 1985.

49. Jaggard, D.L., Hill, C., Shorthill, R.W., Stuart, D., Glantz, M., Rosswog, F., Taggart, B. and Hammond, S., Atm. Env., 15(12), 2511, 1981.

50. Jenzen, J., Appl. Optics, 19, 2977, 1980.

51. Johnson, W.R., Hale, R.W., Nedlock, J.W., Crubbs, H.J. and Bwell, D.H., Tob. Sci., 17, 1973.

52. Kaye, W. and Havlik, A.J., Appl. Optics, 12(3), 541, 1973.

53. Kerker, M., Proceedings of interdisciplinary conference (August 1962), Clarkson College of Technology, Potsdam, N.Y., 1962.

54. Kerker, M., The Scattering of Light and Other Electromagnetic Radiations", Academic Press, N.Y., 1969.

55. Lamer, V.K. and Sinclair, D., "Verification of Mie Theory", OSRD Rep. No.1857 and Rep. No.944; Office of Publishing Board, U.S. Dept. of Com., Wahsington, D.C., 1943

56. Laug, M., Atmospheric Pollution (Ed. Benarie, M.), Elsevier Scientific Publishing Company, Amsterdam, 1976.

57. Lave, L.B. and Seskin, E.P., Air Pollution and Human Health, John Hopkins Press, Baltimore, 1977.

58. Logan, N.A., J.O.S.A., 52(3), 342, 1962.

59. Mandel, L. and Wolf, E., Reviews of Modern Physics, 37(2), 1965.

60. Mercer, T.T., Aerosol Technology in Hazard Evaluation, Academic Press, N.Y., 1973.

61. Mie, G., Ann. Physik, 25, 377, 1908.

62. Muramatsu, M., Umemura, S., Okada, T. and Tomita, H., Envir. Res., 35, 1984.

63. Okada, T., Ishizu, Y. and Matsunuma, K., Beitr. Tabakforsch, 9, 1977.

64. Olaf, J. and Robock, K., Staub. 21(11), 495, 1961.

65. Osher, G., Chem. Rev., 43, 319, 1948.

66. Penndorf, R.B., J.O.S.A., 47(11), 1010, 1957.

67. Penndorf, R.B., J. Phy. Chem., 62(12), 1537, 1958.

68. Penndorf, R.B., Results of an Approximation method to the Mie theory for colloidal spheres, Geophysics Research Paper RAD-TR-59-36, Air Force Cambridge Research Centre, Mass. U.S.A., 1959.

69. Penndorf, R.B., Scattering Coefficients for absorbing and non-absorbing aerosols. Geophysical Research paper RAD-TR-60-27 Air Force Cambridge research centre, Mass. U.S.A. Published by U.S. Dept. of Commerce, Office of Technical Services, Washington, D.C., 1960.

70. Penndorf, R.B., J.O.S.A., 52(4), 402, 1962a.

71. Penndorf, R.B., J.O.S.A., 52(7), 797, 1962b.

72. Perry, R., Hunt, A. and Huffman, D., Appl. Optics, 17, 2700, 1978.

73. Pinnick, R., Carroll, D. and Hofmann, D., Appl. Optics, 15, 384, 1976.

74. Rayleigh, L., Phil. Mag. 12, 81 (Sci. Papers 74), 1881.

75. Rayleigh, L., Phil. Mag., 47, 375 (Sci. Papers, 247), 1899.

76. Rayleigh, L., Phil. Mag., 35 373 (Sci. Papers, 430), 1918.

77. Reist, P.C., "Introduction to Aerosol Science", MacMillan, N.Y., 1986.

78. Repace, J. and Lowrey, A.H., Science, 208, 1980.

79. Rickert, W.S., Robinson, J.C. and Collishaw, N., Am. J. Public. Hlth., 74, 1984.

80 Scott, R.H. and Churchill, S.W., J. Phys. Chem., 62, 1300-1302, 1958.

81. Spencer, D.E., J.O.S.A., 50(6), 584-585, 1960

82. Spurny, K.R. (ed.), Physical and chemical characterisation of individual airborne particles, Wiley, N.Y., 1986.

83. Sterling, T.D., Kobyashi, D.M., Envir. Res., 13, 1977.

84. Steubing, W., Ann Physik, 26(4), 329, 1908.

85. Stevenson, A.F., Heller, W. and Wallach, M.L., J. Chem. Phy. 34(5), 1789, 1961.

86. Stratton, J.A., Electromagnetic theory, McGraw Hill Book Co., N.Y., 1941.

87. Subrahamanyam, V.R., Devraj, B. and Chopra, S., J. Phys. E. Sci. Instrum., 20, 1987.

88. Thompson, B.J., Diffraction and Holographic technique for Practical Size Analysis - a Review, ASME Fluids Eng. Conf. Pittsburgh, Pennsylvania, 1971.

89. Van de Hulst, H.C., Light scattering by small particles, Chapmans Hall, London, 1957.

90. Wattman, W.B., Jr., Cogbill, E.C. and Harlow, E.S., Analyt. Chem. 31, 1959.

91. Went, F.W., Nature, 187, 641, 1960.

92. Wallach, M.L., Heller, W. and Stevenson, A.F., J. Chem. Phy. 34(5), 1796, 1961.

93. Zerull, R., Geise, R. and Weiss, K., Scattering measurement of irregular particles VS. Mie theory, Optical Polarimetry, vol.12, Proc. Soc. Photo-optical Instrum. Enrgrs. 191-199, 1977.